SPACE ENMRONMENT TECHNOLOGIES

UNCLASSIFIED

SET TR 2026-03

SET GOES XRS Solar 0.1-0.8 nm X-Ray Flux Data, 1995 - 2025

S. Dave Bouwer

March 2026

Notice
This document is released for evaluation of SET GOES XRS data. It contains proprietary information to Space Environment Technologies and may not be reproduced without prior written consent by Space Environment Technologies.

SET GOES XRS Solar 0.1-0.8 nm X-Ray Flux Data 1995 - 2025

An SET Composite Historical Database with Daily Background and Hourly Flare indices

Space Environment Technologies Technical Memorandum SET TR-2026-03. Rev. D.

Prepared by: S. Dave Bouwer, Space Environment Technologies. March 11, 2026.

www.spacewx.com

dbouwer@spacewx.com
data@spacewx.com

Table of Contents

Introduction

At Space Environment Technologies (SET), the GOES XRS (X-Ray Sensor) one-minute average of the 0.1-0.8 nm solar X-ray flux is an essential component of several SET data products. This technical memorandum describes the processes developed at SET to convert historical GOES XRS data from satellites GOES-08 to GOES-19 into a single continuous composite time series from the epoch 1995 to 2025.

These data and this technical report are intended for users in the space weather community. The data processing steps, data files, and plots are presented here to describe the scientific and statistical foundation, and the end-to-end data processing and analysis. The composite X-ray flux time series from the each of the GOES satellites is presented so subsequent analysis and models can use a single 0.1-0.8 nm database of one-minute X-ray solar irradiance.

GOES X-ray data products from NOAA tend to emphasize absolute flare irradiances, e.g., flare classifications in W/m^2. In this study, the emphasis is more on the background X-ray fluxes, and the application of hourly flare indices relevant to other hourly and daily solar and geomagnetic indices. The daily background Xb10 and hourly flare indices Xhf & Xhd are derived during the 1995-2025 epoch. These indices are used in the SET products JB08/JBH, SOLAR2000, and the Anemomilos Dst algorithm, and are discussed in greater detail later in this document.

Using the NOAA/NCEI archives (National Oceanic and Atmospheric Administration, National Center for Environment Information), supplemented with the SET operations database, data has been processed to remove erroneous low data outliers, merged using the reference and redundant GOES measurements, and the Xb10, Xhf, and Xhd indices are calculated. NCEI provides an archive of operational data and also science-quality data (*Machol et. al, 2026*). The science-quality data has been reprocessed from operational data and improves calibrations and algorithms. The relative errors between GOES-08 to GOES-19 XRS data are presented, setting the recommended minimum valid flux to 1.2E-7 W/m^2., which is the approximate level suggested by the error analysis and which is the median of the background X-ray flux from 1995 to 2025. Examples are provided comparing the X-ray indices to other solar indices, and illustrating where X-ray flares affect Dst events. The algorithms of this multi-step process will be extended to upgrade the SET real-time X-ray processing algorithms and real-time data products.

GOES XRS Data Overview

GOES X-ray 0.1 - 0.8 nm (1-8 A) flux, in units of W/m^2, is the total solar irradiance from solar coronal emissions from both background full-disk emissions and active-region flares. It has been measured from SMS and GOES satellites since 1974. Solar X-rays primarily affect Earth's ionosphere (D and E-regions), increasing molecular ionization, and resulting in HF degradation/blackouts and satellite communications.

At the NOAA Space Weather Prediction Center (SWPC), the 0.1-0.8 nm X-ray flux is an essential data product used through-out the space weather community, and X-ray flares are events used in mission-critical applications. SWPC is the official distributer of real-time solar X-ray data (https://www.swpc.noaa.gov/products/goes-x-ray-flux). The National Center for Environment Information (NCEI) is the official agency for processing historical measurements and maintaining archives of GOES XRS data. The data downloaded for this study was from the : https://www.ncei.noaa.gov/products/goes-1-15/space-weather-instruments website. The NCEI downloaded data files and documents are included in the SET archives produced by this project. The NCEI GOES XRS "Readme" and Data User Guides may be found at:
https://data.ngdc.noaa.gov/platforms/solar-space-observing-satellites/goes/goes16/l2/docs/GOES-R_XRS_L2_Data_Readme.pdf, and
https://data.ngdc.noaa.gov/platforms/solar-space-observing-satellites/goes/goes16/l2/docs/GOES-R_XRS_L2_Data_Users_Guide.pdf
https://www.ncei.noaa.gov/products/goes-r-extreme-ultraviolet-xray-irradiance.
The Readme document provides the data caveats and tables of the version numbers, while the User's Guide provides the descriptions of the data products. All the data used in this study is from most recent science-quality versions available from the NCEI website (as of Feb. 6, 2026, v 2-2-1). The GOES XRS data provided by SWPC is focused on measuring flares, and official nowcasts are released with the following classifications:

Table 1. X-ray flare classifications.

Flare Class	Flux Threshold, W/m^2
A	1×1.0E-9
B	1×1.0E-8
C	1×1.0E-7
M	1×1.0E-6
X	1×1.0E-5

Additionally, an R-scale classification is used that describes the effects on HF communications:

Table 2. X-ray flare impacts.

Flare Class	Flux Threshold, W/m^2	Impact
R1 (mimor)	1×1.0E-5	Weak/minor HF degradation on sunlit side
R2(moderate)	5×1.0E-5	Limited HF blackout, tens of minutes
R3 (Strong)	1×1.0E-4	Wide-area HF blackout ≈ ~1 hour
R4 (Severe)	1×1.0E-3	HF blackout on most of sunlit side, 1–2 hours
R5 (Extreme)	2×1.0E-3	Complete HF blackout on entire sunlit side, hours

Flare Morphology

Part of the motivation of developing background and flare indices was to create daily and hourly X-ray indices that capture the essential features of pre-flare backgrounds and total flare energies. These indices are components in other SET products. Figure 1 shows a GOES EUV (Extreme Ultra-Violet) image of the sun's corona, in which two major solar active regions are present. In Figure 2 below, an image from SET's Flare Initiation Algorithm (FIA) shows a typical ensemble of minor X-ray flares in relation to the large X-class flare that occurred Nov. 11, 2025. The FIA

algorithm is a unique model that characterizes the beginning, maximum, and flare ending of every flare of any size. It The FIA model was developed by this author in 2011 under contract with the NOAA NESDIS Center for Satellite Applications and Research (“GOES-R XRS.07 Algorithm Test Plan and Results”, Bouwer et.al., 2011). In Figure 2, the pre-flare background is the flux at the moment that occurs just prior to the onset of the flare. But a flare can occur at any time from any visible active region, even when another flare is in progress. In contrast is a background - independent of flares during a day - which would be approximately equal to the lowest pre-flare index in that day, may still have a flare component if there are many flares occurring throughout the day. The FIA model is not elaborated on in this technical document, but is included here to illustrate properties of flares that have an impact on X-ray indices.

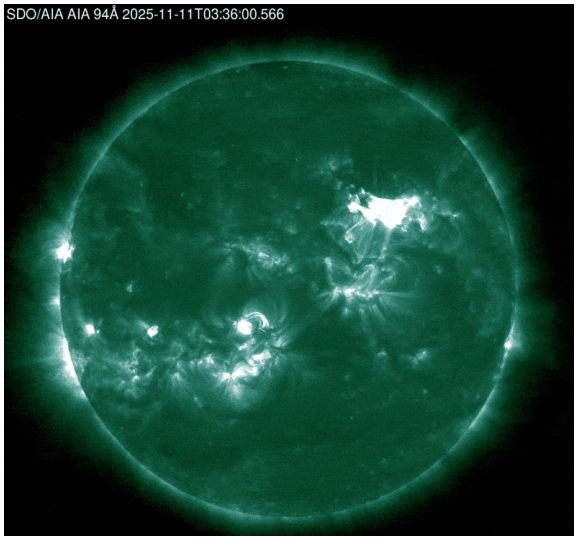

Figure 1. SDO 9.4 nm image during Nov. 11 2025 major solar flare.

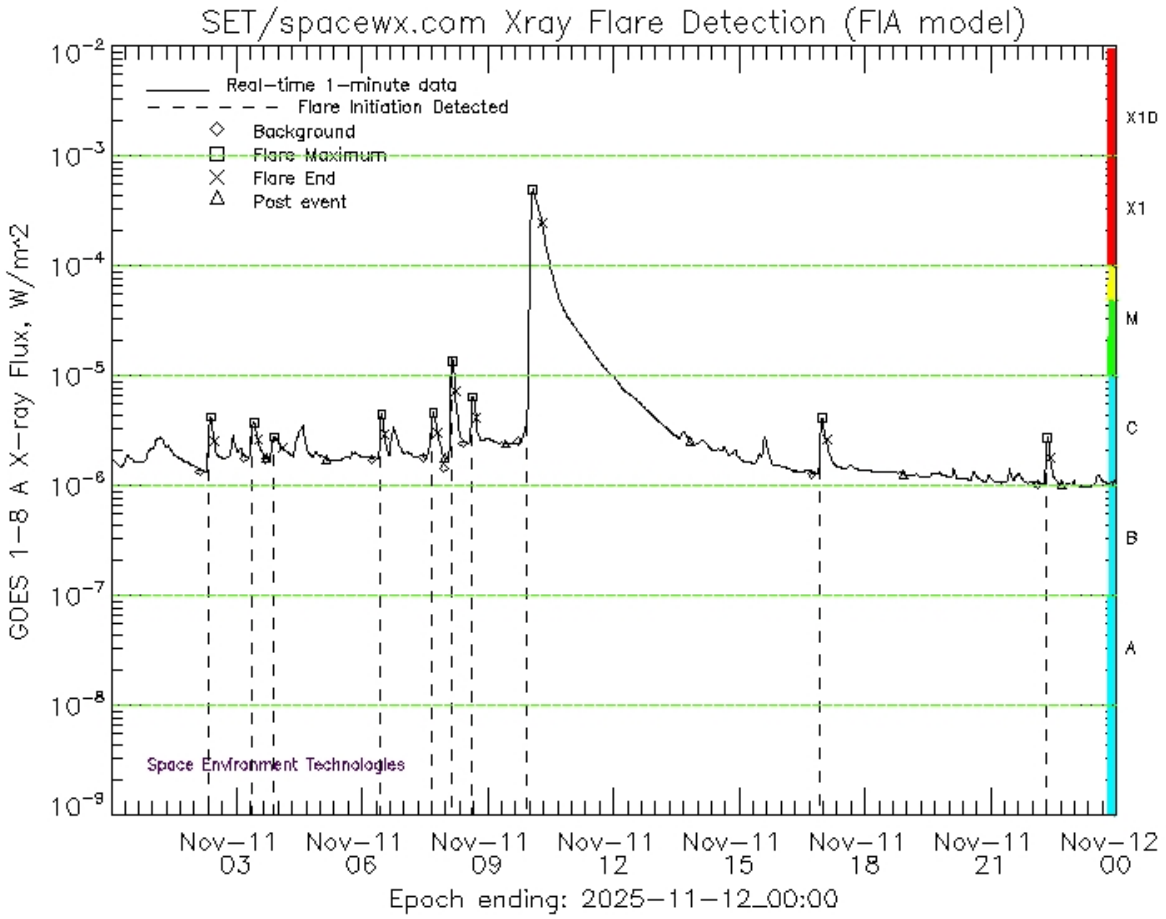

Figure 2. A X-class flare example, produced by the Flare Initiation Algorithm (FIA model).

Processing Goals

At NOAA/SWPC, the focus on X-ray data products is on flare magnitudes, and they announce the real-time maximum flare magnitudes to the space-weather community. In this project, the focus is on X-ray flux backgrounds and relative flare magnitudes. Thus, the final data products are the long-term variability of daily background flux (Xb10), the median hourly flare index (Xhf), and the upper flare index (Xhd). Currently, SET operations produce Xb10 and Xhf data (https://sol.spacenvironment.net/sam_ops/).

In the subsequent analysis, the goal - besides creating a definitive X-ray database - is address the questions:

1. What are the long-term trends in solar X-ray emissions (active region lifetimes to solar cycle epochs)?
2. What are the relative variations of flares with respect to a slowly varying X-ray background?
3. What are the relative errors between GOES 08-19 XRS data?
4. How does solar X-ray irradiance compare to other solar and geomagnetic indices?

Data Challenges

The total number of one-minute data records from 11 GOES satellites prior to creating a composite time series is 25 million. There are approximately 15 million one-minute data records in the final composite time series spanning 31 years. One of the challenges has been to achieve in the data processing algorithms, as closely as possible, 100% accuracy in time series between multiple GOES XRS satellites, creating a montonically-increasing time series with one-minute accuracy. In SET operations, all data records are associated with a YYYYMMDDhhmm time key and a Julian Date. Creating a better than one-minute time grid (date/times and Julian Dates) is essential, and typical algorithms may not address this requirement. For example, in IDL, the JULDAY and CALDAT functions are only accurate to about 10^{-5} seconds, which can accumulate a five-minute error in one year of data. To address this, Java programs were developed using nano-second precision to create a times series 31 years long, resulting in milli-second precision. These Java algorithms have been applied in the code. Of note is that the effect of leap seconds is +-32 milli-seconds each year, but there is an accumulated error of only five seconds between Jan 1, 1999 to Jan 1, 2025. This has a negligible effect in daily and hourly data indices.

Another challenge has been that in periods of solar minimum, GOES XRS measurements fall below the XRS instrument's capability to measure X-ray flux; approximately 5.4E-9 W/m^2 is the absolute minimum. In this report, error analysis estimates the effective minimum valid flux is approximately1.2E-7 W/m^2; below this, the percent error rapidly increase. Error analysis follows in this document. The unfortunate end result of the lower limits of the XRS instruments is that all reliable data is missing or unreliable near and during solar minimum.

Another challenge is data outliers, where the errors can become unacceptably large. Specifically, when the GOES satellite is eclipsed when the Earth obscures the sun, measurements plunge to zero ("drop-outs"). This occurs for up to several hours daily during equinoxes in the fall and spring. And, the XRS instrument takes several minutes to recover after an eclipse. The science-quality GOES data from NCEI has data-quality flags that largely addresses this condition, but the effects of the eclipses still persist to a small degree in the data, and in the real-time data acquired from SWPC. Additionally, there are typical random data outliers from the effects of space-based instruments in the harsh space environment (e.g., cosmic rays and solar energetic particles). Furthermore, some XRS instruments failed to perform properly after launch. However, filtering out drop-outs and consistently using medians and decile algorithms when processing the data the effects of outliers are largely eliminated (Figure 7).

Yet another challenge is the frequent data gaps in the data, where there are times ranging from minutes to years. One of the goals of this project is to combine data from two GOES XRS sources when two sources are available, substituting data from a redundant source when the reference source is unavailable. The final composite time produced by this project is a single time series that is monotonically increasing in time, and portions of the data that are missing are flagged with a missing value flag.

Finally, one of the challenges is that when handling millions of data records, computer performance becomes problematic. Some programs can take up to several hours to run. This condition is addressed by careful programming, and a considerable amount of patience.

Solar Physics Concepts Related to Solar X-ray Flux

Solar Irradiance

The solar irradiance of X-rays is the precise term for what the GOES XRS measures, and it is the total power of 0.1-0.8 nm photons per unit area, and is expressed in units of Watts per square meter (W/m^2). The term solar X-ray "flux", also in units of W/m^2, is typically used in place of irradiance because it commonly is used for describing flare magnitudes and when comparing it to other solar and space weather indices. This report uses the term solar X-ray flux synonymously for solar X-ray irradiance.

In the 0.1-0.8 nm range, one source of "hard" X-rays is from electrons accelerated in the Coulomb fields of ions (free-free Bremsstrahlung radiation), particularly during flares. The other dominant source of "soft" X-rays is from the line emission from highly ionized metals. It is the "soft" X-rays which dominate the background X-ray irradiance.

Solar X-ray irradiance contributes only 10^{-8} to 10^{-5} percent of total solar irradiance. However, it is a relatively significant source of ionization in the Earth's D and E-region ionosphere, although X-rays contribute roughly 10% compared to EUV (Lyman-alpha) irradiance, primarily at altitudes between approximately 60 to 150 km.

Solar X-ray Flare Phenomenology

Solar X-ray flux spans approximately seven orders of magnitude (10^{-9} to 10^{-2} W/m^2), thus a single M-class or X-class flare can be 10^5 times brighter than quiet-Sun values. X-ray flares typically rise from a background to a peak in a matter of minutes (i.e., an impulsive flare event lasting about 3-15 minutes). However, a significant number of flares rise gradually (i.e., a gradual flare event rises more gradually for up to several hours, and can last up to about eight hours). During the impulsive start of a flare, most of the energy comes from the "harder" portion of the spectrum (e.g., 0.05-0.4 nm), and the gradual decline of a flare is in the "softer" portion of the spectrum.

Reference in the literature is often made to "micro-flares"; which occur at that the 10^{-8} W/m^2 level and are associated with small, localized reconnection. Moderate active-region flares (C-class) begin at about 10^{-8} to 10^{-5} W/m^2 and are coherent active-region events, and large flares begin at about 10^{-5} to W/m^2, (M & X-class) and are associated with major magnetic restructuring, and are often associated with coronal mass ejections (CME).

Ionospheric Effects

There are numerous technologies affected from ionization in the D and E regions of the ionosphere: HF radio blackouts, GNSS/GPS accuracy, VHF/UHF satellite links, aviation navigation, radar systems, and more. Solar X-ray flares are a space-weather hazard with measurable impacts on national infrastructure and commercial operations. Many effects are more due to EUV changes, but X-rays are a reasonable proxy to some EUV effects. However, even after a large X-class flare, the ionosphere can recover in under an hour to pre-flare conditions.

Solar Rotation and The Center-to-Limb Effect

The generally cited estimate for an active region to appear to rotate around the sun is 27 days, but this is a somewhat inaccurate view. Because of the suns differential rotation, active regions can appear to rotate about the sun at different periods: The 27.3-day period is associated with active regions near 0 degrees latitude, the 28.2 day period with active regions near 30 degrees latitude, and the 30.0 day period is associated with 60 degrees latitude (*Bouwer, S.D, 1983*).

There are typically more than one active region randomly distributed in longitude about the Central Meridian Distance (CMD) at 0 degrees (0 degrees longitude is the center of the sun as viewed from Earth). Additionally, active regions evolve over about 3-5 solar rotations, rapidly becoming active, then gradually declining (*Bouwer, S.D. 1983*). As a result of differential solar rotation and active region evolution, *observed* solar-rotation periodicities observed from Earth can appear to be as little as 20 days, and as long as 36 (*Bouwer, S.D., 1992*).

The center-to-limb effect arises from solar rotation and the opacity of the sun's outer layers (transition region to lower corona). The sun's outer coronal atmosphere is optically thin to X-rays. Contrast this to the chromosphere (e.g., measured by Mg II c/w, Ly-a), which is more optically thick. Thus chromospheric irradiances appear as a sine wave over a solar rotation, but X-rays will appear as more of a square wave. Additionally, in X-rays, active regions appear at the limbs 1-2 days before and after chromospheric plages are visible. This has an impact, for example, when performing a least-square regressions of solar X-ray flux to other solar indices like Ly-a or Mg II c/w (Magnesium II center-to-wing ratio near 280 nm).

In the time series analysis of solar indices, these effects are typically mitigated in time series data by averaging time series over 27 days to highlight active regions, and 81-days to reduce the effects of active region evolution in the time series. Nevertheless, when comparing the background Xb10 index to chromospheric indices like Mg II or Ly-a, there will be a lot of scatter about the mean due to the CMD effect. Interestingly, the often-used F10.7 index contains both chromospheric and coronal components, making it an only an approximate proxy to either chromospheric or coronal indices (Figure 22).

Often sudden increases in X-rays are associated with CME's (Coronal Mass Ejection). But the CMD dependence of both CME's and X-ray active regions result in a poor correlation. CME's are typically only geoeffective if they erupt between about 30 degrees East to 45 degrees West of the CMD. Thus, to the degree a flare is associated with a CME - which in itself is not apparent without the active region latitude and longitude - a large flare can occur near the sun's limb and no CME will be detected.

One interesting result from this project is that often, when there is a geomagnetic event at Earth, there is a second or third - order effect observable in the Dst index, where if a flare occurs during the Dst event, there is a small change in the hourly Dst (Figure 25).

The X-ray index, Xi

X-index Definition

Throughout the data processing in this project, the X-ray index "Xi" is used. This is calculated using the formula:

$$Xi = 100 * \log_{10} \left(Flux\left(\frac{W}{m^2}\right) * 10^{10}\right)$$

To convert Xi back to flux units,

$$Flux\left(\frac{W}{m^2}\right) = 10.0^{(\text{ (Xi -1000.0) / 100.0 })}$$

This is used for several reasons. It was originally introduced by Dr. Richard Donnelly at the NOAA Space Environment Center around 1978 as a convenience when comparing X-ray data to other solar indices, such as F10.7. It was used to determine the daily background index Xb by this author to describe intermediate-term epochs in 1983 (Bouwer, S. D., 1983). It can be conceptually viewed as doing X-ray data calculations in "log-space". It has a number of attributes, especially when computing statistical properties, e.g., when calculating the Root-Mean Square Error (RMSE). It is also a technique used in other fields such as earthquakes or sound intensity. It is a statistical technique that aids in comparing variability over flux decades, evaluating flare statistics, or studying correlations between in indices. The net result is that in examining relative changes in X-ray flux, the changes are equally weighted in between decades. The contrast between using arithmetic versus logarithmic error analysis are as follows.

Arithmetic RMSE:

- Dominated almost entirely by large flux values (C-, M-, X-class).
- Completely insensitive to accuracy during quiet periods.
- RMSE becomes essentially a "flare-error metric," not a general metric.

Logarithmic RMSE:

- Weights all decades of flux equally.
- Quiet-Sun A & B-classes, and C, M, X flare-class differences all contribute proportionally.
- Produces a much more stable and interpretable statistic.

Thus when converting X-ray flux into a logarithmic index ("log-space"), basic statistics (e.g., medians and percent errors) are more meaningful, and are relatively more comparable to other arithmetic indices. For example, statistical normality is achieved when index units are used in linear regressions of GOES X-ray data between two satellites when the regressions are done in log-space (Bouwer et. al., 1982), and this fact is the basis for the error analysis the follows (Table 3).

SET X-ray Applications

Solar X-ray Indices

In many applications, solar and geomagnetic indices are daily or hourly. In the SET LEO Alert & Predictions System (LAPS), which is based on the JB2008/JBH09 HASDM model (*Bowman, B.R. 2008*), four daily solar proxies are used: S10, F10, M10, and Y10. Y10 is a combination of the Ly-a solar flux and the solar X-ray Xb10 daily background (https://spacewx.com/jb2008/). Additionally, the SET Anemomilos Dst forecast uses the solar X-ray hourly flare indices (https://sol.spacenvironment.net/sam_ops/current_data/Dst_streamB_forecast.jpg).
Another application is the characterization of X-ray flares in the SET FIA model, which identifies the onset and maximum of flares:
(https://sol.spacenvironment.net/sam_ops/current_data/GNN_XRS_FIA_out.jpg).

But most importantly, the role of solar X-ray flux in describing solar variability is its role of describing the sun's corona, as compared to the chromospheric indices Mg II or Ly-a, or the F10.7 cm solar radio flux at 2800 MHz. Time series of the daily Xb10 varies very differently than daily chromospheric indices or F10.7 (Figure 22).

Simply doing statistical means of X-ray flux in units of W/m^2 heavily biases results to flares, obscuring the properties a background solar variability, thus the development of the X-ray indices Xi and Xb10. Furthermore, in this project, nearly all statistical calculations and derivation of X-ray indices, the median, not the mean, is used. This is done to mitigate the bias of flare maximums and to address the inevitable outliers in the one-minute data: just a single X-ray value can bias an hourly or daily index if it is a decade or more above or below the adjacent values in the time series and a mean is used. For example, when calculating the average X-ray flux above a daily background, if the interval being used has several values more than a decade below the majority of data in that hour due to the GOES satellite being eclipsed by the Earth and the XRS instrument has not recovered to its normal temperature range, the mean of hourly or daily estimates will result in very incorrect value. A median value will mitigate this erroneous condition. Under normal circumstances, the mean and median will be nearly identical. By way of analogy, one would not calculate average monthly wind speed in by including hurricanes.

Daily Background Index Xb10

The principal motivation behind the development of a daily background index Xb10 is two-fold: first, to have a daily index to compare to other daily solar indices that is unaffected by flares, and secondly, to have a basis for calculating flare activity above the background. This has the consequence that, for example, an X4 flare at 10^{-4} W/m^2 above a 10^{-5} W/m^2 background is much smaller then a an X4 flare at 10^{-4} W/m^2 above a 10^{-6} W/m^2 background, by an order of magnitude.

A daily background index Xb was first introduced by this author in 1982 in a NOAA/SEL Technical Memorandum (Bouwer et. al., 1982), using a simple algorithm that used the lowest of three eight-hour bins within a day. It was done at a time when computer resources were limited and many calculations were still done by a hand calculator or using a Fortran program on a computer mainframe. Beginning about 2004, this author developed an improved daily background

for operational use; Xb10 (Bouwer, 2006). Figure 3 illustrates how Xb10 consistently is lower than Xb.

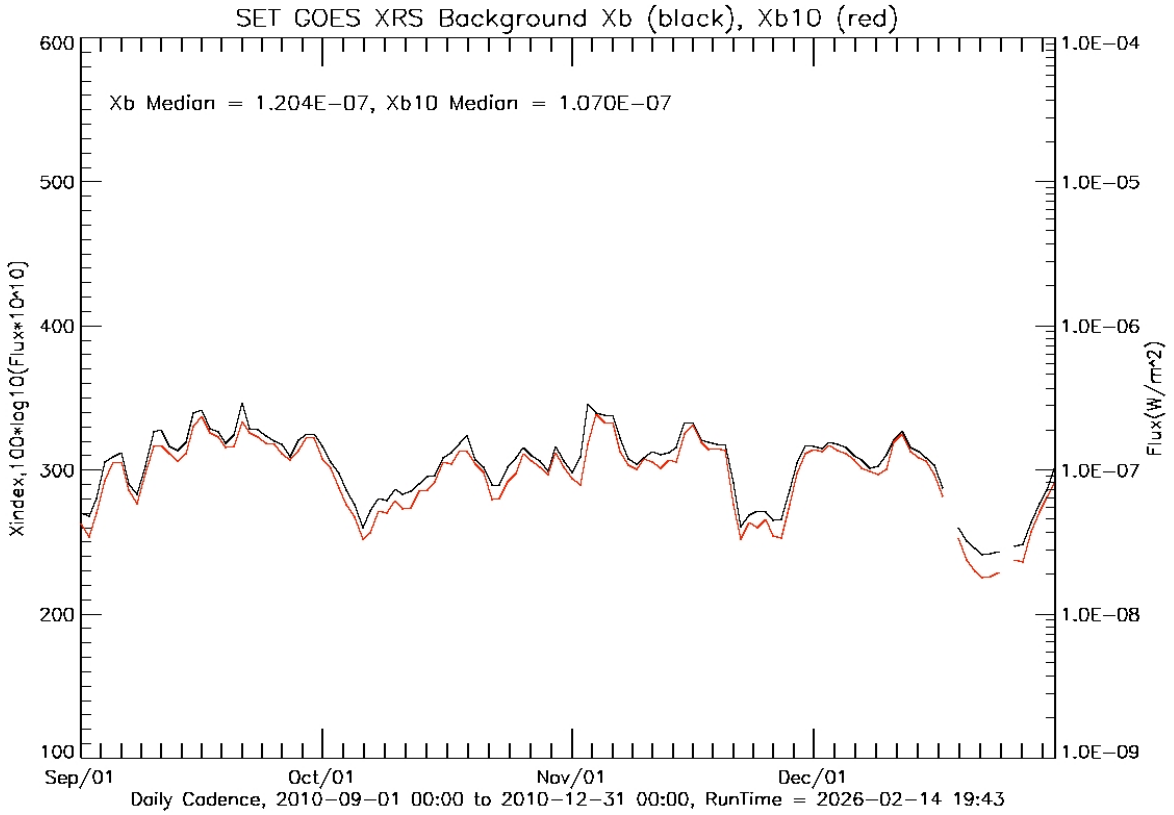

Figure 3. Comparison of the daily background indices Xb to Xb10.

The Daily Xb10 index is defined as the median of the 60 one-minute Xi values within the *lowest*-flux hour of each day. For each day, the 1-minute Xi data are grouped into 24 hourly bins; the hour with the lowest central tendency is identified, and the median of its 60 samples is reported as Xb10. Although not accurately a statistical decile, Xb10 is conceptually similar to the median of the lower hourly decile.

Using the median of the lower hourly bin mitigates the effects of anomalous low outliers. In Figure 4 below, an example is shown for 2024, during solar maximum of solar cycle 25. Xb10 during this period show the combined effects of multiple active regions and solar rotation.

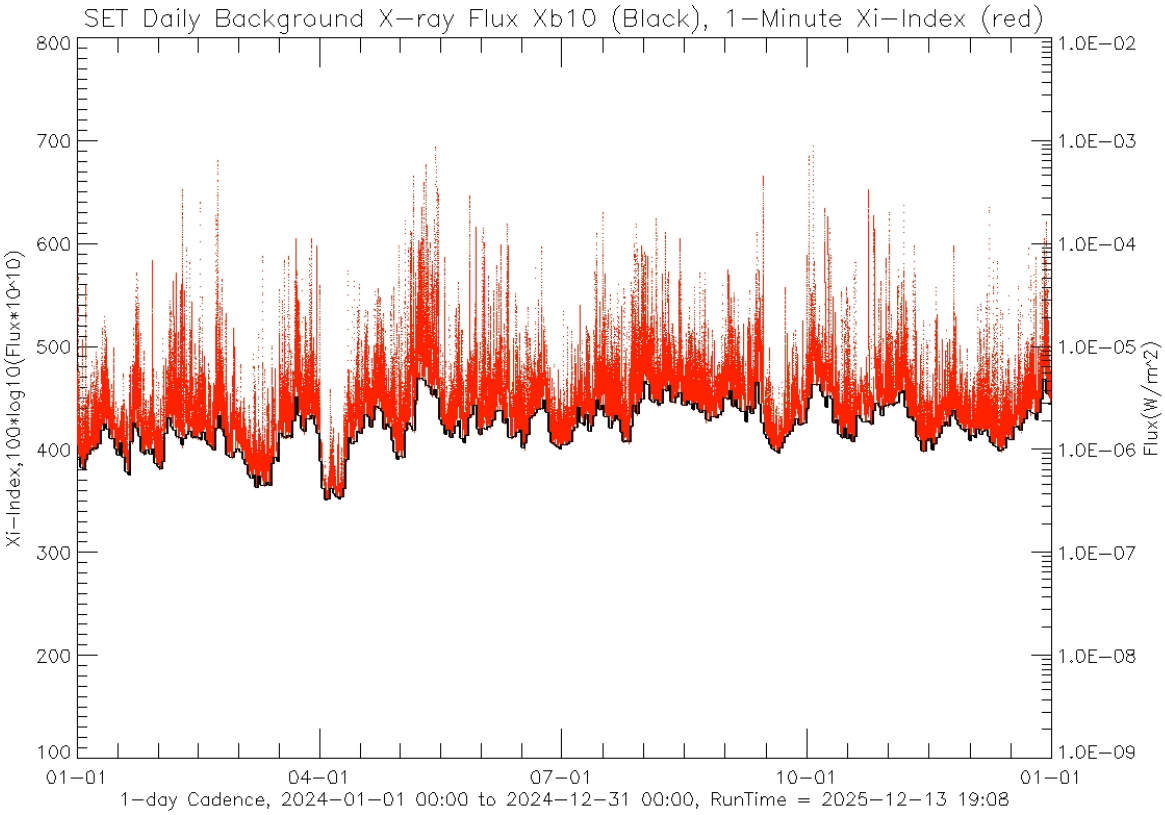

Figure 4. An example of the 2024 daily Xb10 index and one-minute X-ray flux.

Simply calculating a daily mean or median of X-ray flux in W/m^2 units is mis-leading: large flares dominate the calculation during active times, obscuring the overall level of activity. By selecting just the median of the lower hourly bin of one-minute data, a more meaningful index of background variability is derived.

The Hourly Flare Index Xhf

The Xhf hourly flare index is defined as the median of the 60 one-minute Xi values within the hour of each day *above* the daily background index Xb10. For each day, the 1-minute Xi data are grouped into 24 hourly bins; and the median of its 60 samples is reported as Xhf. By using the median flux within an hour of above each day's background helps ensure that low data outliers are not affecting the result, albeit there may be slightly lower values within a day. The Xhf index is weighted towards the soft X-ray portion of the spectrum.

The principal motivation behind the development of Xhf is for applications that need an hourly flare index, in particular, the Kent's (Tobiska et.al, 2013) Anemomilos model that uses hourly Dst data. By consistently using Xhf across all time epochs, consistent comparisons can be made.

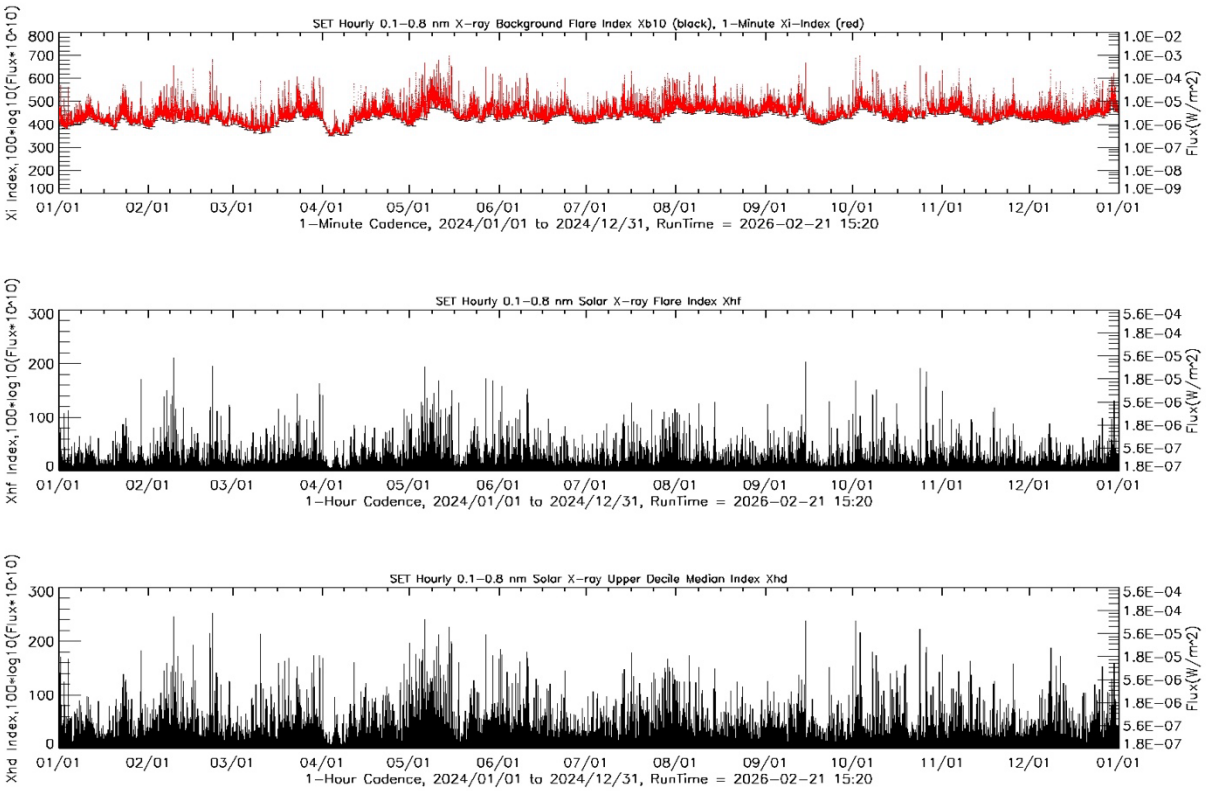

Figure 5. An example of the 2024 hourly flare indices Xhf and Xhd.

To calculate the flux in W/m^2 above Xb10, add Xhf (or Xhd) to Xb10, then convert that to total flux in W/m^2, then convert Xhf to flux, then difference them, e.g.,

1. Xsum = Xb10 + Xhf
2. FluxSum = 10.0^((Xsum -1000.0) / 100.0)
3. Fluxhf = 10.0^((Xhf-1000.0) / 100.0)
4. FluxDiff = FluxSum - Fluxhf

FluxDiff then is a proxy index to the total energy over an hour above the daily background, which is an approximation, not the more accurate total integrated flux derived by summing all the one-minute flux above the pre-flare background.

The Hourly Flare Index Xhd

The Xhd index is a new SET data product, introduced in this document. The Xhd hourly flare index is defined as the median of the highest 10% of one-minute Xi values within each hour above the daily background Xb10. For each day, the 1-minute Xi data are grouped into 24 hourly bins; the 60 one-minute values within each hour are sorted, and the median of top 10% of samples is reported as Xhd. While this index does not capture the maximum of a flare, it is weighted more towards the hard X-ray portion of the spectrum, and captures more of the accumulated flux above the background over and hour. Xhd is conceptually similar to the median of the upper hourly decile (thus the “d” in Xhd).

Xhd is always between slightly above Xhf to considerably higher. For example, a flare can range from a short high burst of X-ray flux, on the order of less than 10 minutes (in which case Xhf will be enhanced, but Xhd will be nearly the same as Xhf) , to a large flare that evolves of hours (in which case Xhd will be much larger than Xhf). Consequently, it more accurately represents the input energy to the ionosphere's D and E-region ionization above the slowly-varying background. This has implications to HF radio communications and GPS accuracy due to increases to the Total Electron Content (TEC), among other potential technologies.

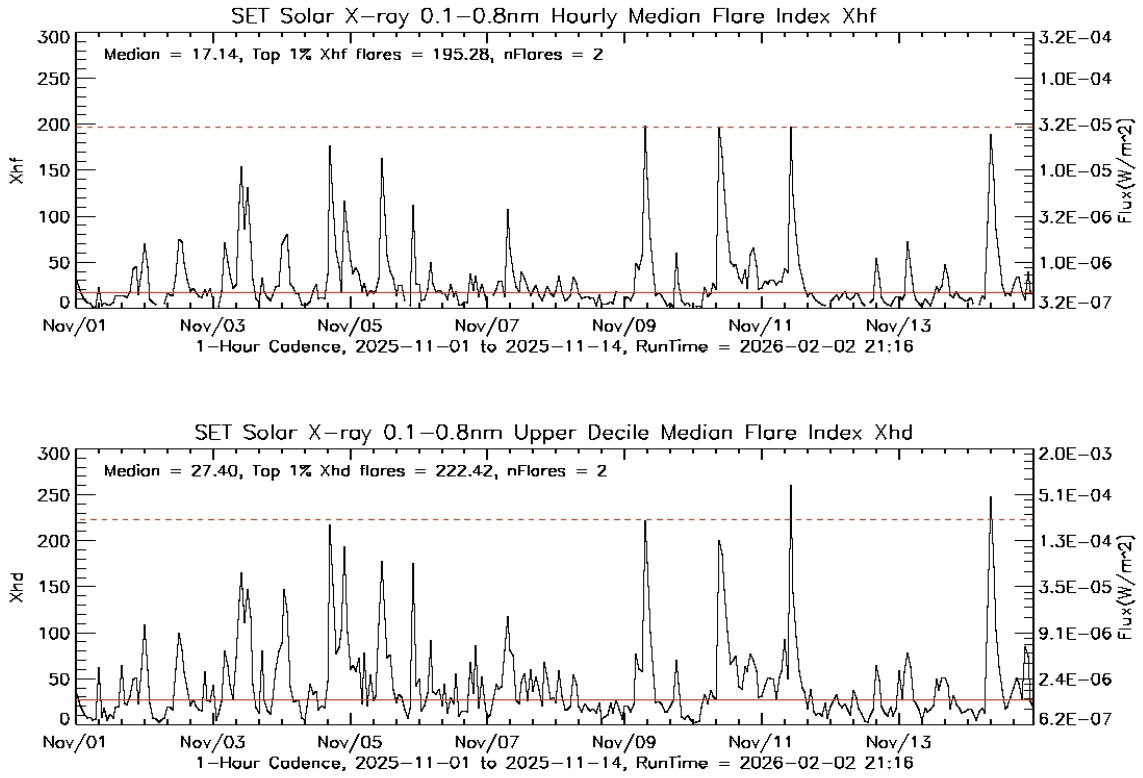

Figure 6. The Xhf and Xhd indices, November 1-15, 2025.

Figure 6 shows the Xhf and Xhd indices for the November 1-14 time period, when there were multiple large flares from two large active regions, most notably an active region in the northwest quadrant of the sun near (N23, 03-23W). From the medians (Xhf: 17.14, Xhd: 27.40) it is apparent that X-ray flux is dominated by small flares. But the three major flares between Nov. 9-11 were all X-class flares, lasting over three hours each. The Nov. 9 flare was associated with a massive CME-related geomagnetic event Nov 12 - among the largest in decades - when aurora were visible as far south as Florida and South Texas. In a later discussion in this report Xhd is shown to have a direct relationship to the hourly Dst.

GOES XRS Data Assimilation

Ingesting GOES XRS data from multiple sources and processing them into a value-added time series is the first step in this project. It is challenging because of the dramatic volume of data (over one-half of a million data records per year), and because of the idiosyncrasies of real-time data (data gaps, drop-outs due to the GOES satellite view of the sun being eclipsed by the Earth, particle contamination, merging data between two GOES spacecraft, etc.).

The GOES-XRS data for this report comes from two sources: The NOAA/NCEI NetCDF files (GOES-08 to 18), and from SET's real-time database, which is downloaded from NOAA/SWPC on an hourly basis (GOES-19). Note that GOES 18, & 19 data is collected at SET and stored in the SET database hourly, and published at https://www.swpc.noaa.gov/products/goes-x-ray-flux.

It is relatively straight-forward to download the NetCDF-formatted files from NCEI and decode the data to an ASCII-formatted file. However, the subsequent processing requires careful attention to details, and considerable code was written, tested, and applied to accomplish this task

NCEI Data Archives and Decoding NetCDF files

The science-quality historical X-rays data archived at NCEI can be found under the NOAA/NCEI link:
https://www.ncei.noaa.gov/data/goes-space-environment-monitor/access/science/xrs/.
The files are in NetCDF format, and must be decoded. The Java class Read_GOES_xrs_cdf.java program was used to extract the data (the /set_lib/netcdfAll-5.8.0.jar lib must be in the Java classpath). It is a component of the Xray_1min_Assim.java main driver, which also calls the Java class Update_hist_1min_DB.java, which subsequently stores the data in the MySQL database.
A valuable utility is the Panoply application available from NASA/GISS; it was used to examine the metadata and data values to code and validate Read_GOES_xrs_cdf.java. The NCEI NetCDF filenames look like: sci_xrsf-l2-avg1m_gNN_yYYYY_v1-0-0.nc.

Only three fields are extracted from the NetCDF file: time, xrsb_fux, and xrsb_flag, using statements like: timeVar = CDFdataFile.findVariable("time"), timeArray = (ArrayDouble.D1), timeVar.read(). See the in-line comments in the Java class Read_GOES_xrs_cdf.java for more details. The xrsb_flag is a bit-masked field, which when converted from an unsigned short, yields the flags "bad_missing_data", "eclipsed_by_earth", etc. These flags are used to assign a missing-value flag to the X-ray measurement that is stored in the SET database. The "time" attribute in the CDF file is the number of seconds since 1970 for data prior to the year 2000, then the number of seconds since the year 2000. The java classes EpochSecs_to_YMDhm*.java performs this conversion.

The data time series are guaranteed to be time-monotonic (no gaps or duplicates) between the beginning and ending times. The background and flare indices are in Xi units, and can be converted to W/m^2 units by applying the equation shown below. It is important to note that when Xb10 = 100.0, it signals a missing-value flag (this avoids taking the log of zero or a negative value). The missing-value flag for the Xhf and Xhd indices is 0.0.

The composite database begins with GOES-08 on 1995-01-03_00:00 and ends with GOES-18 &19 on 2025-12-31_23:59. Note there is one data gap in the composite database:

- Between the end of GOES-10 (2010-12-31) and the beginning of GOES-15 (2011-01-01), data are unavailable.

There are other intermittent missing data at other times (i.e., one of the GOES satellites has missing data and there isn't a redundant GOES satellite data value available at that time), so those are flagged in the database with Xi = 100.0. During solar minimums (approximately 1996, 2007, 2008, 2009, 2018, 2019), data from the XRS falls below the lower limit the instrument can measure i.e., Xi ~= 175. Thus, there are long periods during solar minimum where there are missing data. A missing-value flag (Xi=100.0) is substituted into the time series as a missing-value flag in those cases as well.

XRS Data Processing

Date/Time Usage

A long-time SET convention for representing date/time data is using the YYYYMMDDhhmm format, as opposed the ISO standard YYYY/MM/DDtHH:MM.SS.xxx. YYYYMMDDhhmm is a useful format because it is a single field in code and databases, can be converted to a computer Long, is easily sorted, and can easily be converted to a format consistent with ISO or SQL formats by parsing the field with substring methods (e.g., YYYY-MM-DD hh:mm). All SET date/time records are in UTC units. This data format is used throughout the code and as the primary key in the SQL database. When used in conjunction with the Julian Dates field to select subsets within the time series, exact precision can be achieved in identifying a specific one-minute record or range of records (e.g., selecting an hour in a day).

Data Processing Steps

In processing the data from NCEI CDF files to a useful data archive spans the following overall steps:

1. Downloading CDF files from NCEI for each GOES satellite (GOES-08 - GOES-18) and year, decompressing the data, creating 1-minute time keys and Julian Dates for each record, storing the data in the SQL database, and providing plots and data files for initial verification. For GOES-16 - 19, the real-time SET database can be used directly.
2. Retrieving data from the database, inserting data into a time-monotonic grid, removing leading and trailing sections of missing or invalid data, rejecting data that falls below the XRS data limits, calculating basic statistics (e.g., mean, median, standard deviations), and creating files of hourly and daily medians.
3. Filter data to remove the data dropouts due to the GOES satellite being eclipsed by the sun-earth positions during equinoxes, interpolating over small time gaps after removing outliers, then storing the processed data in the SQL database.
4. Comparing concurrent measurements between GOES satellites, determining which GOES-NN XRS data will be reference/redundant data sources preparing the data for subsequently merging, and calculating error statistics.

5. Merging the data from the assorted GOES satellites into one time-monotonic time series, storing the data in the SQL database, organized by year.
6. Calculating the daily X-ray background Xb10 and hourly Xhf & Xhd flare indices, storing the data in the SQL database. This is the database that all subsequent programs and analysis use. Plots and data files, organized by year, are produced.
7. Subsequent analysis compares Xb10, Xhf, and Xhd indices to the F10.7 data, producing plots and files of particular interest, highlighting major flare events, and comparing Xb10 to the Ottawa F10.7 time series, and comparing Xhd to a major Dst event in November, 2025.

It is important to note that the calculations are of the entire time series from 1995 to 2025; and is based on nearly 13 million one-minute records, 22,000 one-hour records, and 9,000 daily records, so the figures below provide only a rough overview. More detailed images are included in the appendices, and over 200 detailed plots and data files are available online (Appendix A. SET X-Ray Data Archives").

Outlier Filtering

Due to a number of GOES XRS instrument anomalies (e.g. eclipses), there can be sudden "drop-outs" where the data falls far below adjacent flux levels. Using the data quality flags in the NCEI CDF records, a large majority of these erroneous data are removed. However, there remain a very small number of instances where a dropout is still present or a random contaminated one-minute measurement is present, and in real-time operational data (e.g. GOES-18 &19) acquired from SWPC. In this projects data processing, to filter out extreme outliers, daily median outliers are first removed in the cases where a daily median data value falls below 2.5 standard deviations from neighborhood values. In the second stage of processing outliers, a statistical algorithm (using the IDL Moment function) uses a kurtosis algorithm of the lowest median, iteratively removing values until the kurtosis approaches an acceptable threshold near zero. In Figure 7 below, this is illustrated for GOES-19 (which is pending revision by NCEI). In the top panel, the dropouts are highlighted with a symbol showing where the daily median of 1-minute data falls. The bottom panel show the result of applying the kurtosis algorithm. Filtering out dropouts helps to ensure that subsequent daily background Xb10 values are unaffected by these extreme outliers. Extreme upper outliers have not been filtered out, but because median values are used in background Xb10, Xhf, and Xhd, upper outliers have no effect.

In nearly all calculations the median - not the mean - is used when using subsets of the time series, mitigating the negative effects of outliers and the way large flares can bias the means, medians, standard deviations, and percent errors. Also, the Xi units are used so differencing calculations can be done in "log-space". This approach, combined with using the subset medians of flux data (e.g., hourly flare indices), provides proxy indices to the average properties of daily and hourly fluxes not dominated by extreme values.

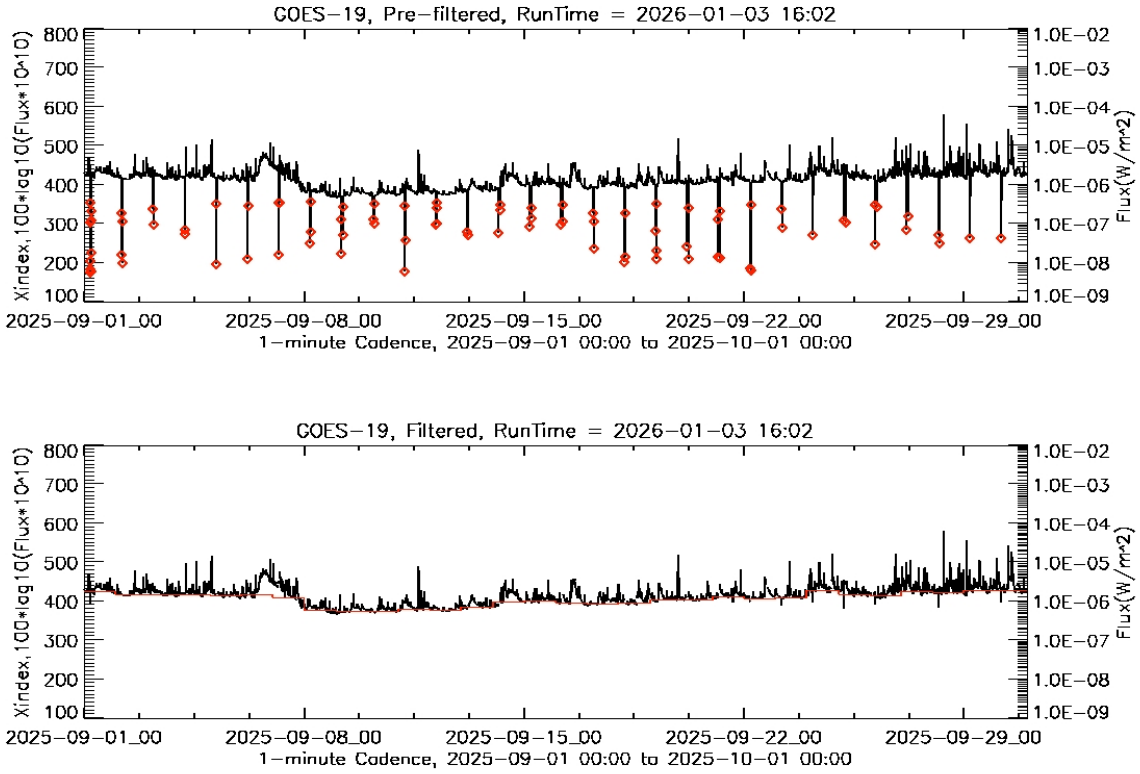

Figure 7. Demonstrating the effects of dropouts on daily medians and the results of a kurtosis filter algorithm.

Error Analysis

In the discussion below, comparing data between two satellites produces shows relative (percent) errors over different X-ray flux decades. This was done by first calculating the difference of the medians of each source and applying the offset to one of the sources (this was only a minor adjustment in most cases). Then, doing a basic linear correlation to reduce long-term biases, and plotting the scatter diagram and residuals. The RMSE is calculated from the residuals. The detailed comparisons are shown in Table 3 below.

GOES Satellite Comparisons

In Figure 8 below, one of the best-case comparisons is shown; GOES-08 vs GOES-10. These data show a consistent correlation, except for very small differences in a narrow range between 300 < Xi < 400 during 1999-2000 possibly due to the responsivity differences of the XRS detectors (Mothersbaugh, 2023). The RMSE over the entire range of Xi is 1.1355 Xi-units.

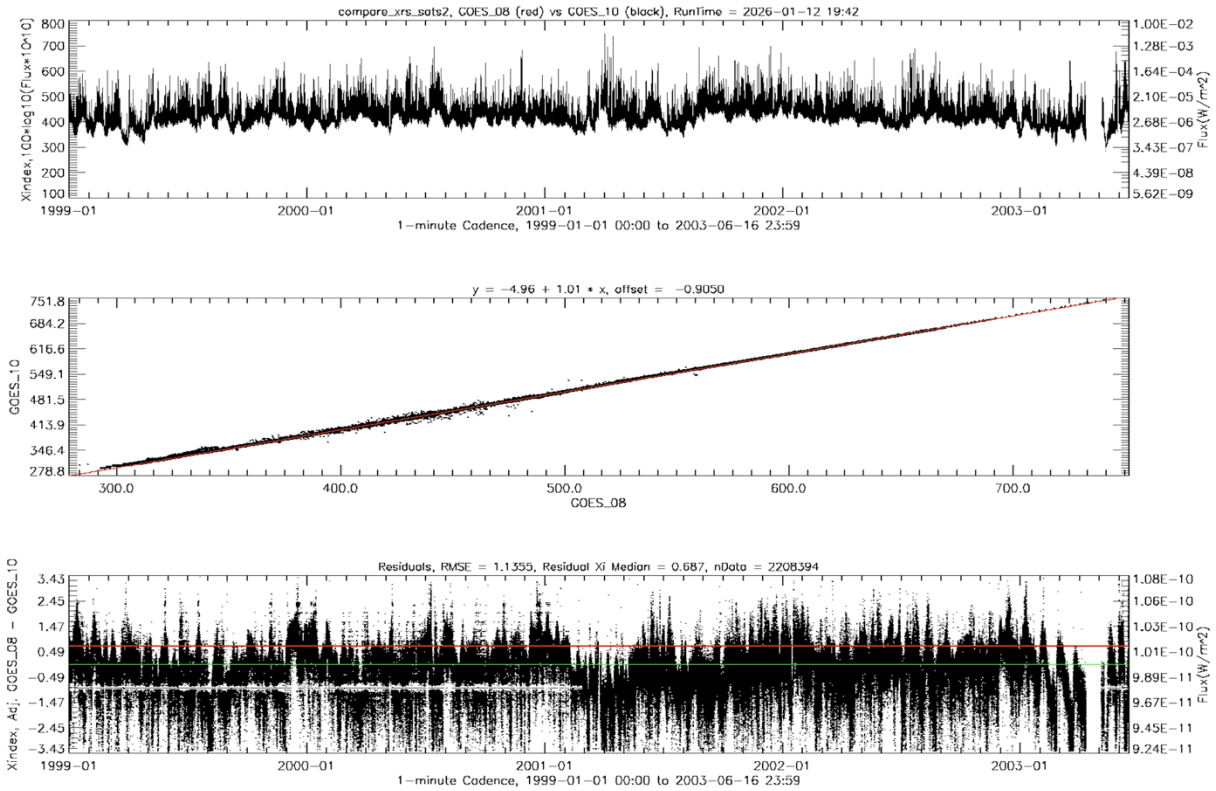

Figure 8. GOES-08 vs. GOES-10 for entire flux range.

To clarify the errors in the 300 < Xi < 400 range, the RMSE is calculated just for that one decade. In Figure 9 below the errors are better illustrated. In that case, the RMSE decreases to 0.663 in Xi units, or 4.6% percent error in W/m^2 units (Table 3).

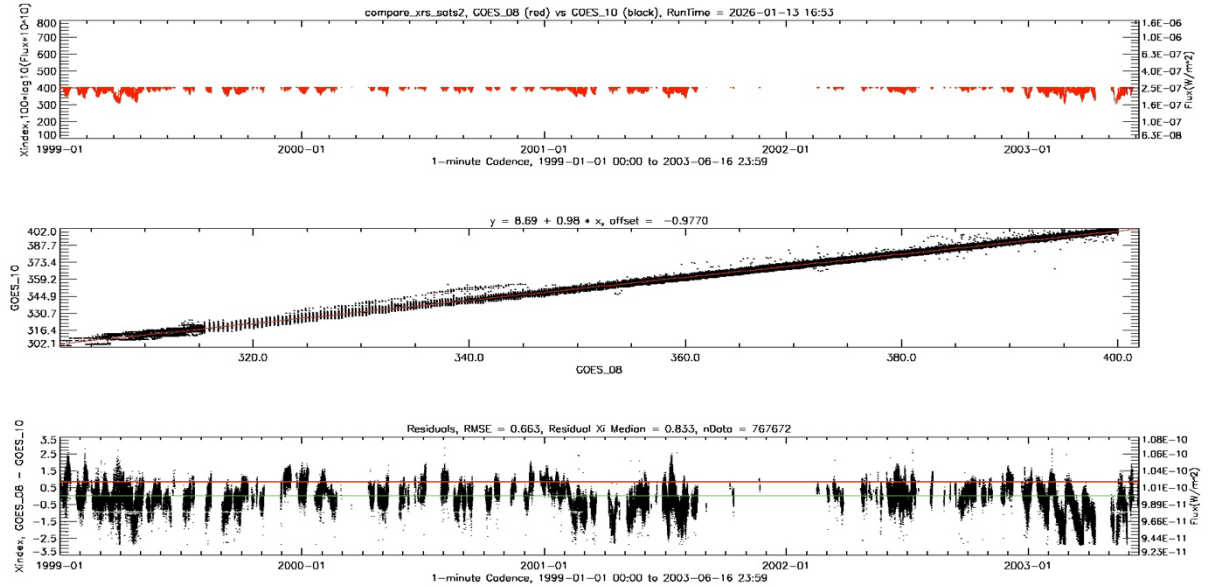

Figure 9. GOES-08 vs.GOES-10 for flux corresponding to 300 < Xi < 400.

In contrast, calculating errors between GOES-15 to GOES-16 shows much larger errors at low flux levels (Figure 10). This low-flux effect is present in all comparisons, effectively setting a lower accuracy limit, approximately at Xi = 330 (1.2×10^{-7} W/m^2). In most cases, data below Xi = 300 (1.0E-7 W/m^2) has a percent error > 100%.

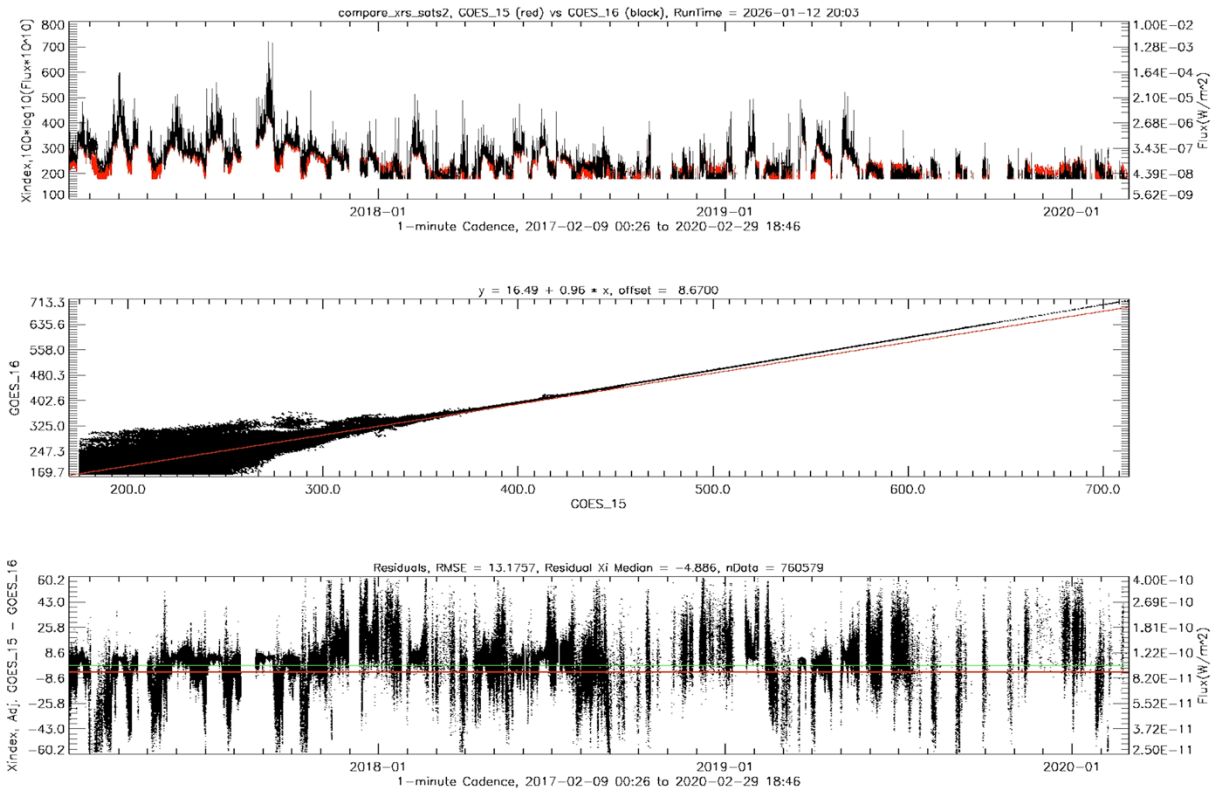

Figure 10. GOES-15 vs. GOES-16, 175 < Xi < 800.

These calculations are done in "log-space" using the Xi index, in order to underscore the relative variability within each flux decade. In Table 3, the first column shows the two satellites used with concurrent data, between the indicated X-index ranges. The second column shows the offset applied to bring the medians the same between the two time series. The third column shows the Root Mean Square Error (RMSE) in X-index units. The fourth column shows the average percent error (PE) within that decade in W/m^2 units (%PE = RMSE^10). What is apparent in nearly all cases, the higher the flux, the smaller the PE error. For GOES-08 and GOES-10, the percent errors are quite small. But for GOES-12, 15, 18, and 19 the percent errors are significantly larger. In general, below Xi = 350 (3.2E-7 W/m^2) the percent error rapidly increases. This suggests that the daily background Xb10 below 350 is increasingly in error. At about Xi = 300 (1.0E-7 W/m^2), the percent errors exceed 100% and that data should not be used for analytical purposes.

There was one instance when the comparison between two GOES satellites indicated highly erroneous results: GOES-09 vs GOES-10 in 1998. In Figure 11 below, it is clear that there is no correlation between the two sets of measurements. In comparisons between GOES-08 and GOES-10, there is no issue. Consequently GOES-09 was not used as part of the composite database.

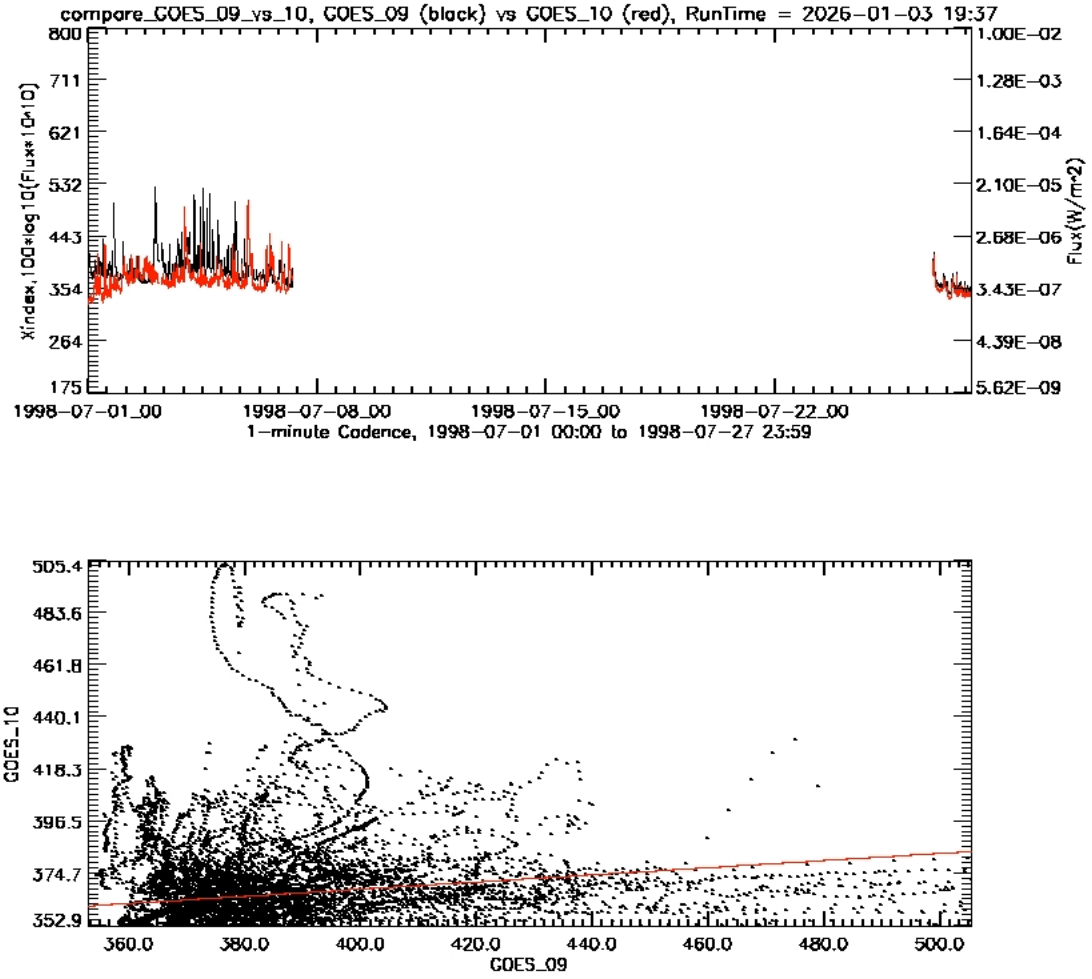

Figure 11. GOES-09 vs. GOES-10 showing large errors.

RMSE and PE of GOES XRS Comparisons

As mentioned earlier in this document, a Root-Mean Square Error (RMSE) is calculated over each decade. Calculating the RMSE over all decades somewhat over-estimates percentage errors. But calculating the RMSE separately for each decade mitigates the effect of large flux values biasing the percentage error. Still, it is not a linear relationship. In Figure 12 below, the Percent Error (PE) is shown, in log-space, in relation to the RMSE. Thus the %PE shown in Table 3 below, calculated from the RMSE^10, is an approximation of the lower portion of the curve in Figure 12. However, if consistently applied to each decade when comparing GOES satellites, the RMSE and PE provide a useful error estimate.

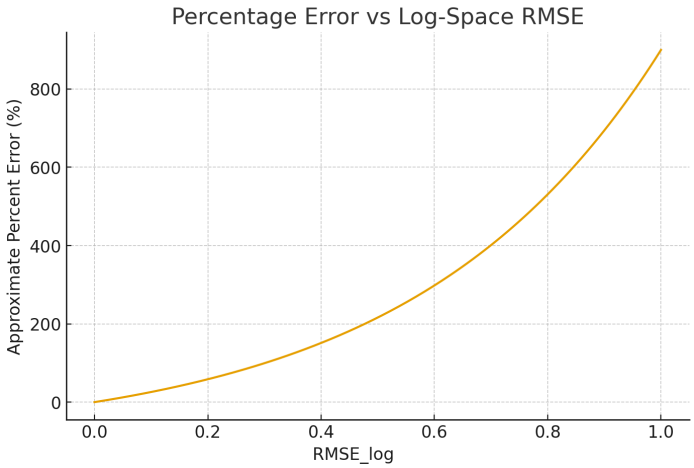

Figure 12. The relationship between the Percentage Error vs Root Mean Square Error in log-space.

Table 3. Error analysis.

	Offset	RMSE	%PE
GOES_08_vs_10_200_800	-0.905	1.136	13.68
GOES_08_vs_10_350_800	-0.921	1.107	12.79
GOES_08_vs_10_200_300	Insuf.Data	Insuf.Data	NA
GOES_08_vs_10_300_400	-0.977	0.663	4.60
GOES_08_vs_10_400_500	-0.857	0.841	6.93
GOES_08_vs_10_500_600	1.613	0.327	2.12
	Offset	RMSE	%PE
GOES_08_vs_12_200_800	0.000	1.191	15.52
GOES_08_vs_12_350_800	-0.175	0.630	4.27
GOES_08_vs_12_200_300	Insuf.Data	Insuf.Data	NA
GOES_08_vs_12_300_400	0.000	1.093	12.39
GOES_08_vs_12_400_500	-0.386	0.376	2.38
GOES_08_vs_12_500_600	0.000	0.139	0.00
	Offset	RMSE	%PE
GOES_10_vs_12_200_800	1.660	5.242	>100
GOES_10_vs_12_350_800	0.386	0.818	6.58
GOES_10_vs_12_200_300	-0.350	5.347	>100
GOES_10_vs_12_300_400	1.384	1.588	38.73
GOES_10_vs_12_400_500	-0.624	0.495	3.13
GOES_10_vs_12_500_600	-1.489	0.193	1.56
	Offset	RMSE	%PE
GOES_13_vs_15_200_800	1.140	5.698	>100

GOES_13_vs_15_350_800	0.517	1.157	14.35
GOES_13_vs_15_200_300	-0.350	5.347	>100
GOES_13_vs_15_300_400	1.118	1.556	35.97
GOES_13_vs_15_400_500	-0.298	0.667	4.65
GOES_13_vs_15_500_600	-4.561	0.395	2.48
	Offset	RMSE	%PE
GOES_15_vs_16_200_800	4.585	7.694	>100
GOES_15_vs_16_350_800	3.281	0.600	3.98
GOES_15_vs_16_200_300	5.354	7.468	>100
GOES_15_vs_16_300_400	4.058	1.511	32.43
GOES_15_vs_16_400_500	3.102	0.317	2.07
GOES_15_vs_16_500_600	3.159	0.118	1.31
	Offset	RMSE	%PE
GOES_16_vs_18_200_800	-0.050	0.685	4.84
GOES_16_vs_18_350_800	-0.050	0.683	4.82
GOES_16_vs_18_200_300	Insuf.Data	Insuf.Data	NA
GOES_16_vs_18_300_400	-0.793	0.432	2.70
GOES_16_vs_18_400_500	-0.048	0.503	3.18
GOES_16_vs_18_500_600	-0.399	0.095	1.24
	Offset	RMSE	%PE
GOES_18_vs_19_200_800	-1.076	2.230	>100
GOES_18_vs_19_350_800	-1.069	2.195	>100
GOES_18_vs_19_200_300	Insuf.Data	Insuf.Data	NA
GOES_18_vs_19_300_400	-2.139	1.835	68.39
GOES_18_vs_19_400_500	-0.629	0.983	9.62
GOES_18_vs_19_500_600	0.432	0.098	1.25

In Table 3, it can be seen that with the exception of GOES-15 vs GOES-16, the offsets between satellites is relatively small. The goal of this analysis was not to alter the calibrated NCEI versions of XRS data, but to simply clarify the relative errors, so offsets were not applied to data in the final database. However, low outliers are either marked with missing-value flags, or if a redundant source is substituted in when the reference data point falls well below the redundant source. The offsets and percent errors between GOES-15 vs GOES-16 are relatively large until Xi > 400, so it appears the GOES-15 XRS instrument suffers from a degree of inaccuracy. Similarly, the percent errors between GOES-18 vs. GOES-19 are relatively large until Xi > 450 (Figure 14).

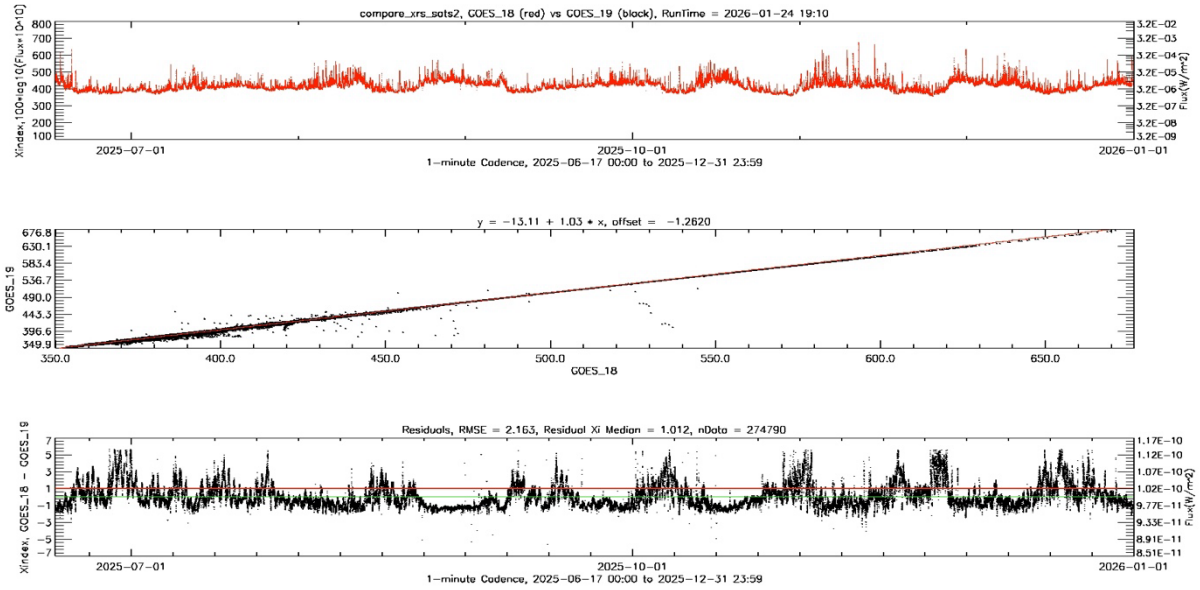

Figure 13. GOES-18 vs. GOES-19, 200 < Xi < 800.

Examining the GOES-18 vs. 19 one-minute Xi errors closer, it becomes clearer where the 68% percent error (in W/m^2 units) comes from: At low flux levels (300 > Xi <400) there is considerable scatter and biases. The GOES-16 to GOES-18 data look good, so the implication is that the GOES-19 XRS data is suspect at low flux levels.

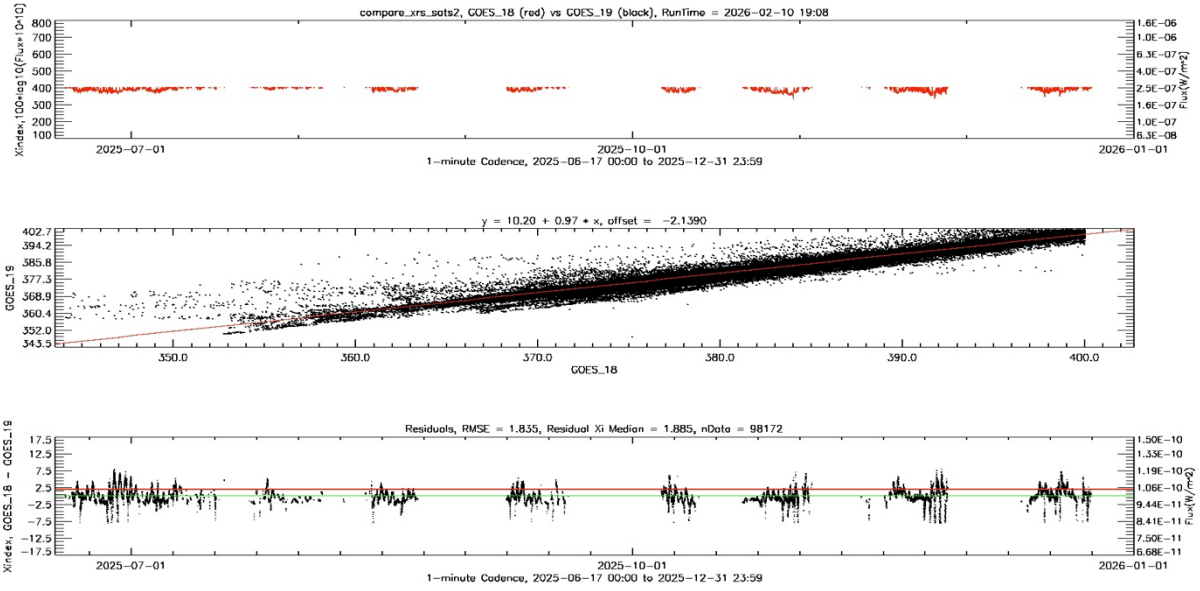

Figure 14. GOES-18 vs. GOES-19, 300 < Xi < 400.

Error Analysis Summary

One of the goals of the error analysis is to determine at what level can one safely assume the relative errors are acceptable for all the one-minute data for analytical calculations. While each GOES XRS instrument has its unique limitations, from Table 3 it can be seen that between 300 < Xi < 400 all the percent errors all fall below 100%. Coincidently, Figure 17 shows the median of Xb10 from 1995 to 2025 is nearly equal to 330, or 1.2E-7 W/m^2. Thus, for reliable analytic purposes, as a "rule-of-thumb", Xi = 330 or 1.2E-7 W/m^2 is the recommended minimum flux. Below 1.2E-7 W/m^2, errors rapidly increase in the one-minute flux data.

GOES-09 was not used in the final composite because of obvious errors. GOES-11 was not used in the final composite time series because GOES-10 and GOES-12 already provided sufficient coverage during 2006. In the case GOES-14, the data were so sparse, at low flux levels, or with high relative errors they were not included in creating the composite time series. The end result is the reference satellites in this project are GOES 10, 15, 16, and 18. The redundant satellites substituted into composite time series when the primary had no data are GOES-08, 12, 13, and 19. An illustration of the reference and redundant GOES XRS datasets is shown in Figure 15.

Finally, it is important to note that despite all the algorithms applied to remove outliers, there are still a tiny percentage of one-minute outliers in the data, but less than roughly 0.001%. An additional sidebar is that when the recent issued GOES-16 & 18 data were compared to the SET real-time database, the differences were relatively small (<1%) until Xi began to become lower that 400, where the differences increased, but the background and flare indices were relatively unaffected when Xi > 300.

The SET GOES XRS Composite Time Series

One of the main goals of this project is to create a single, time-monotonic time series of one-minute X-ray flux that can be used to create the Xb10, Xhf, and Xhd indices.

In Figure 15 below, a table of the reference and redundant GOES satellites over time is illustrated. These were the GOES satellites used to create the composite database. The green rows show the reference satellites, the yellow rows show the redundant satellites. Note that the references to "reference" to "redundant" is not the same as the NOAA "primary" and "secondary" designations. The choices of reference and redundant were made based on the interpretations from the error analysis and the duration of the time series. The bottom two roles indicate the approximate part of the solar cycles at minimum, ascending/declining, or solar maximum. The beginning and ending dates are also indicated. Note the four-month gap between 2009-12-01 to 2010-09-01, during which there were no reliable data near solar minimum. Additionally, there are very little data in 2008 and 2009 during solar minimum.
Also note that GOES-08 to GOES-18 are based on the latest NCEI NetCDF files (as of February 2026), but the GOES-19 data are from the SET real-time database, which acquired the real-time data from SWPC.

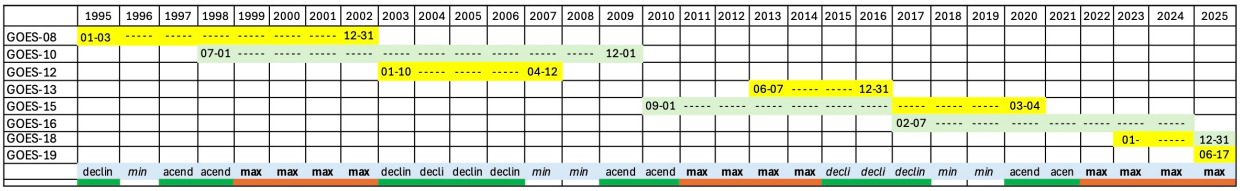

Figure 15. Summary of which satellites were used to create composite time series.

When merging data from two concurrent GOES XRS datasets, gaps in the reference dataset can be filled in from the redundant dataset, at approximately hour 09 UTC, as illustrated in Figure 16. Additionally, there are many instances where the flux from the reference data is significantly lower than the redundant data. When merging data from two GOES satellites into one composite the RMSE is used. If, at one point in time, an XRS measurement from one GOES data value is greater than another by Xi_sat1 - RMSE × 10 > Xi_sat2, the Xi_sat1 value is used in the composite (the RMSE of 350 to 800 is used). This addresses the unusual instances when one XRS measurement is still a significant low outlier, especially during eclipses and solar minimum conditions. At high levels of flux (e.g., Xi > 500), the relative errors are so small that differences are insignificant.

However, there is still the open question of what is the "truth" calibration for all the satellites. In the composite created by this study, offsets have not been applied, maintaining the absolute values from NCEI science-quality data unique to each satellite.

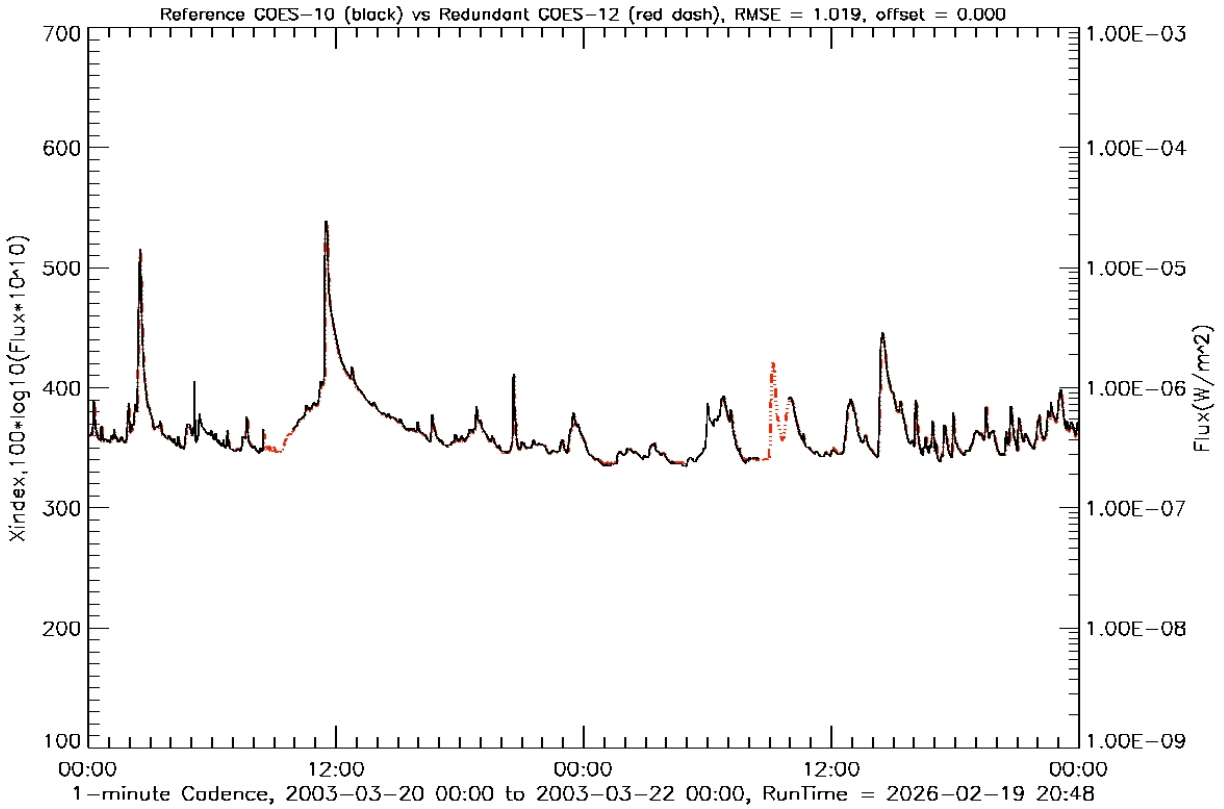

Figure 16. Example where the reference satellite (GOES-10) missing data near 09 UTC is supplemented from the redundant GOES-12.

Once the one-minute composite database was completed, the next step was to calculate the Xb10, Xhf, and Xhd indices and store them in the SQL database. The key step is first calculating Xb10, after which the Xhf and Xhd indices are calculated and stored in the database.

Properties of the Xb10, Xhf, and Xhd Indices

The SET Xb10 background is designed to remove the effects of solar flares, capturing active regions coronal X-ray flux modulated by solar rotation. The SET Xb10 daily background index differs from the SWPC background index issued as one of its data products. One motivation behind developing a new background index Xb10, instead of using the minimum of a daily 8-hour bin developed in 1981, was to have an X-ray metric more comparable to other solar indices (e.g., F10.7, Mg II c/w, geomagnetic indices, etc.), and for better estimating the relative increase of flares above the background X-ray flux. If one uses a mean value over a day or hour, the result would be one where the data was heavily biased by flares, and the result would be a time series poorly correlated to other daily solar time series indices. In contrast, the Xb10 daily background is heavily weighted towards a lowest decile median, resulting in a daily background significantly less than the SWPC Xb version. This results in a more accurate daily background and flare indices, uncontaminated by data outliers.

In the figures below, it is important to recall that the entire 31-year time series is based on nearly 13 million 1-minute records and 22,000 1-hour records, so the figures provide only a rough overview (there are only so many pixels per inch). More detailed files of over 500 detailed plots and data files are available from SET online archives, as described in Appendix B.

Xb10 , Solar Cycles 22, 23, 24, 25

In Figure 17 below, Xb10 is shown for solar cycles 22 to 25. The Xb10 data from 1986 to 1994 was acquired from an earlier study, and are included here for illustration. While Figure 17 illustrates the solar-cycle in log-space and the solar cycle maximums appear nearly equal, it is worth recalling that in terms of the relative increase in flux W/m^2 units, there is a 900% increase in flux from 1.0E-7 W/m^2 to 1.0E-6 W/m^2. Furthermore, note that because the GOES-R XRS instruments (GOES-16, 18, 19) are unable to accurately measure solar flux below about 5.6E-8 W/m^2, and are increasingly inaccurate below 1.0E-7 W/m^2, the lower portions of the ascending and descending solar cycles are inaccurate (Table 3). The quiet-sun background 0.1-0.8 nm flux is unknown, although it has been estimated to be ~(1-3) × 10^{-9} W/m^2 from early SOLRAD data (*Kreplin, R. W., Taylor, J. A., 1970*).

In Figure 17 are five-year lines centered about solar maximums above the overall medians of the daily background Xb10 for solar cycles 22 to 25. Note the 60% (in W/m^2 units) decrease in solar cycle 24 maximum median at Xb10 = 371 (5.2E-7 W/m^2) with respect to solar cycles 22, 23, and 25 solar cycle maximum medians, which are nearly identical at approximately at Xi = 390 (7.9E-7 W/m^2). In the bottom panel of Figure 17, a 365-day Hanning filter was applied to emphasize the long-term trends. A Hanning filter is a weighted moving-average filter that applies a raised

cosine window, giving greater weight to the center of the window and tapering smoothly to zero at the edges.

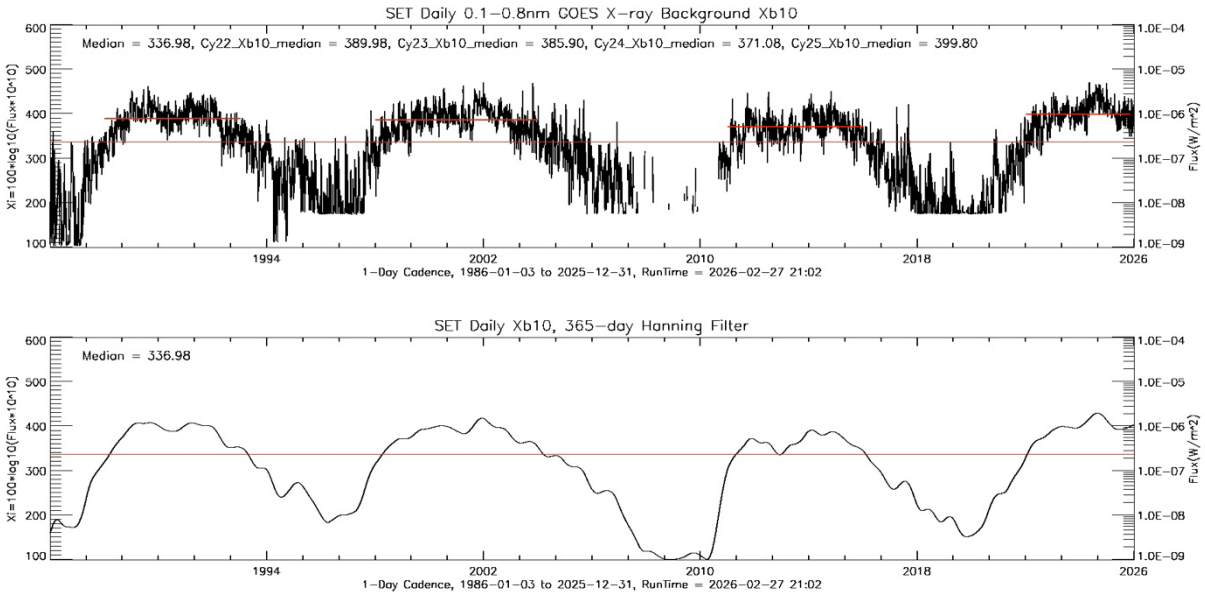

Figure 17. The Daily X-ray Background Xb10, 1986-2025.

Xhf and Xhd Flare Indices, Solar Cycles 23, 24, 25

In Figures 18 and 19 below, the Xhf and Xhd time series are shown for 1995 to 2025. Of particular note is the variation of the medians of Xhf during solar cycles 23, 24, and 25 maxima. Solar cycle 23 has a maximum of median Xhf = 127, cycle 24 of 132, and cycle 25 of approximately Xhf = 125. The number of flares in top 1% percentile is 2,333.

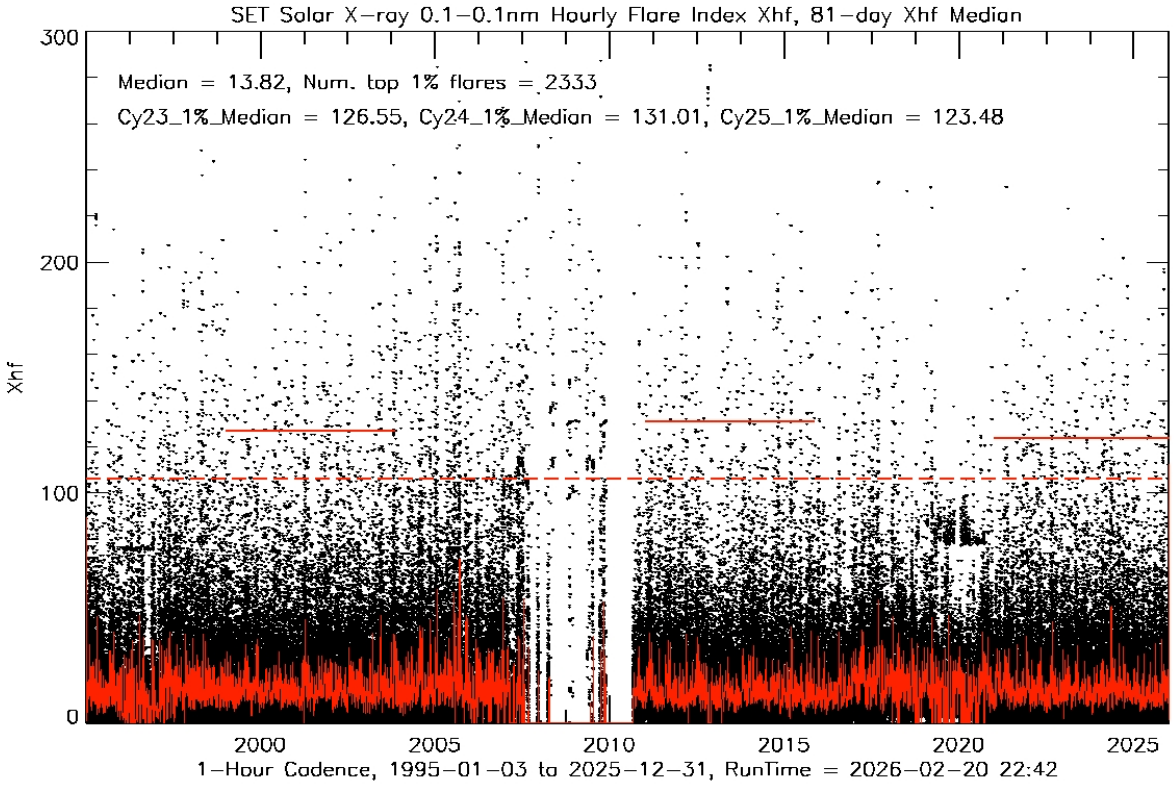

Figure 18. The hourly X-ray flare index Xhf, 1995-2025.

A similar result is observed in using the median of Xhd, which is heavily weighted towards total flare flux above the daily background. Solar cycle 23 has a maximum of median Xhd = 169, cycle 24 of Xhd = 173, and cycle 25 of Xhd = 167. Again, the results suggest the cycle 24 flares are larger than cycle 23, and cycle 25 flares are lower than cycle 23. One would expect that flares exhibit similar behavior independent of the solar cycle. Perhaps there is a mis-calibration of the XRS-B instruments between GOES-08, GOES-15, and GOES-16 in the GOES XRS-B detectors. In other words, there might be too many X-class flares reported during cycle 24, and there might be too few X-class flares reported during cycle 25. Or, it may be an effect of the 22-year Hale cycle; but there is insufficient long-term X-ray data to clarify solar cycle dependencies.

The number of flares in top 1% percentile is 2,306, which is nearly the same as the Xhf case of 2,324.

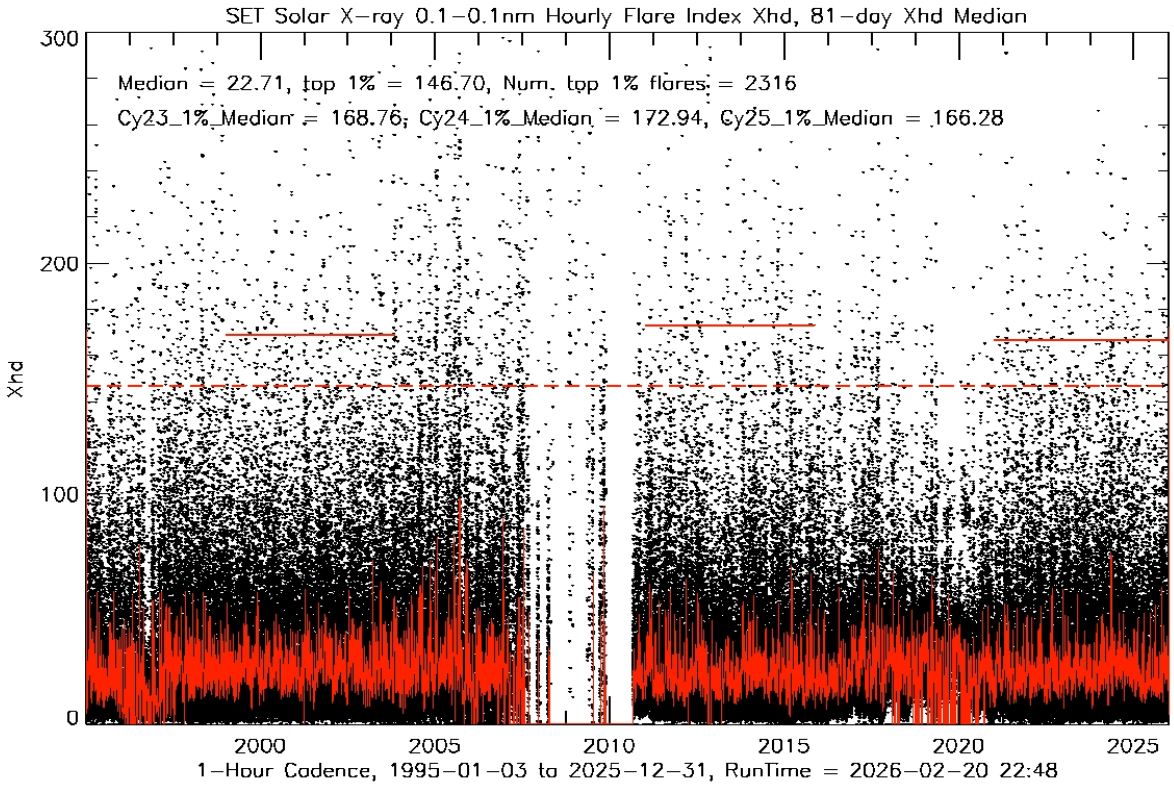

Figure 19. The hourly X-ray flare index Xhd, 1995-2025.

Distribution of Flare Indices

The distribution of flare indices is of interest. The intensity of flares has been associated with minor flares related to localized reconnection, or moderate active-region associated with coherent active-region events, or large flares associated with major magnetic restructuring. One might expect some sort of discreet distribution as a result. But when the distribution of flare indices is shown (Figure 20, Figure 21) both Xhf and Xhd show a smooth distribution. This could be further investigated by examining the FIA database.

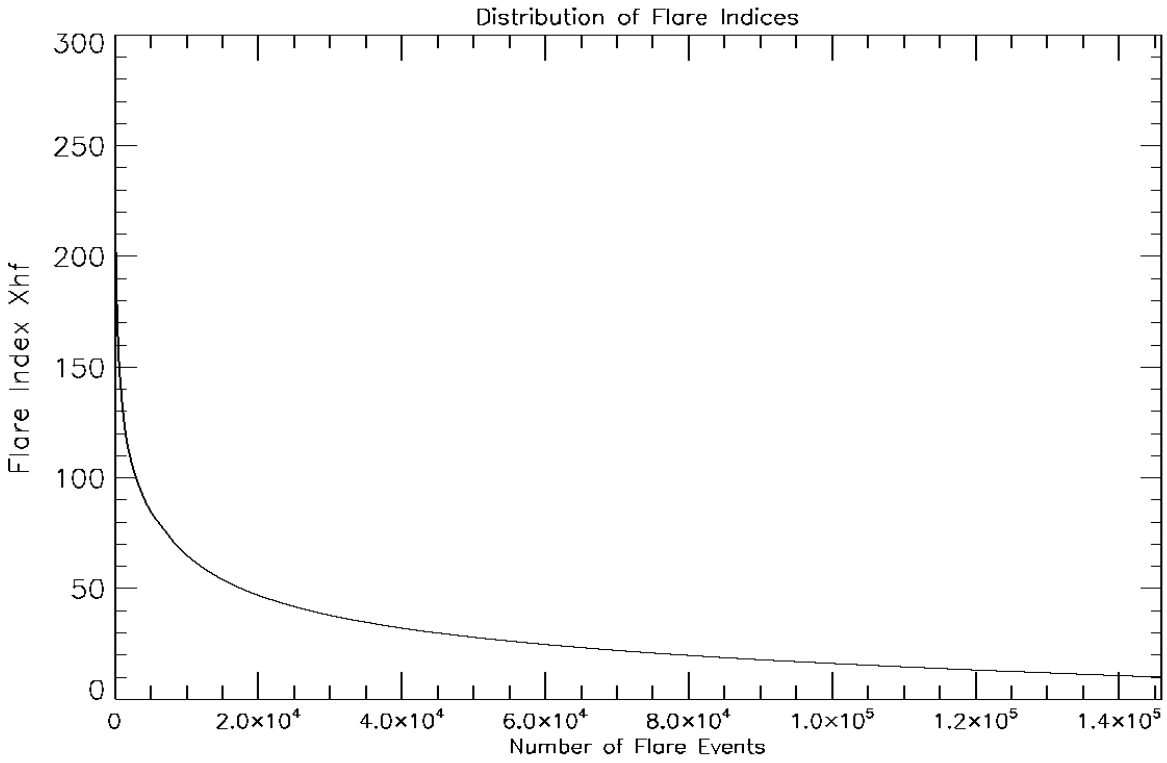

Figure 20. Distribution of hourly flare indices Xhf, 1995-2025.

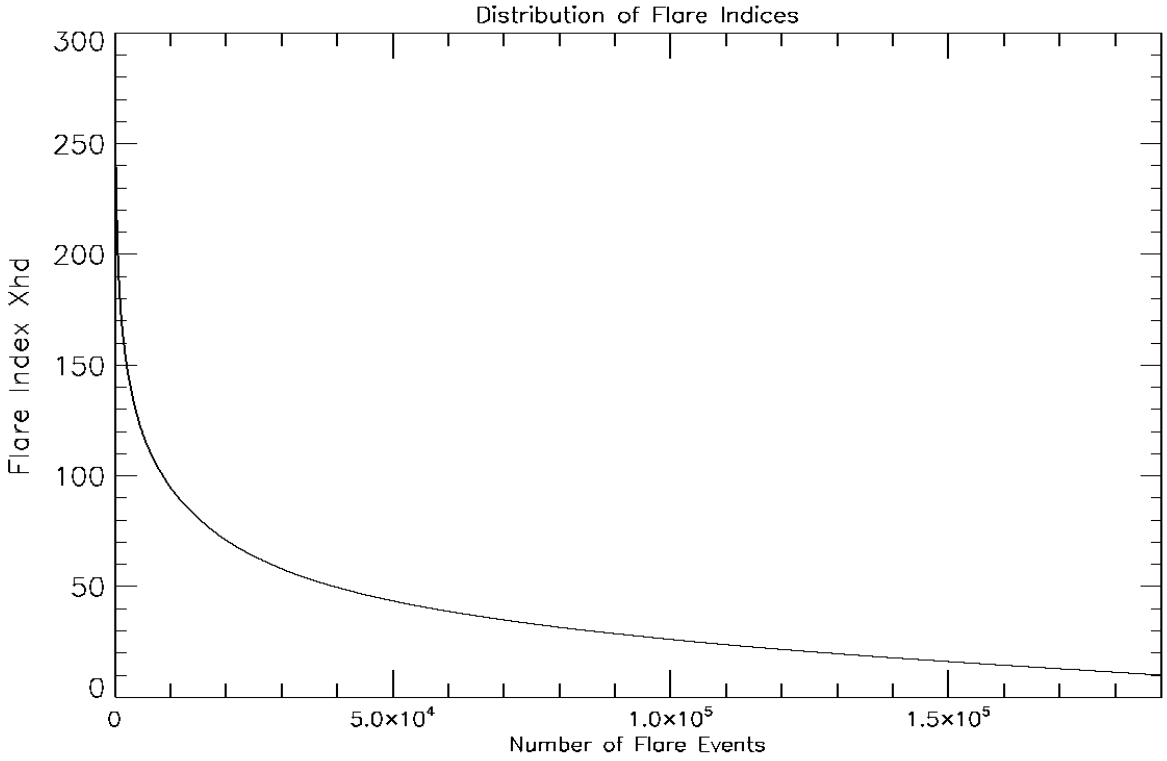

Figure 21. Distribution of hourly flare indices Xhd, 1995-2025.

Xb10 Compared to Solar Indices

Below in Figure 22, several solar indices are normalized to illustrate how they vary with respect to each other. Comparisons are made between the coronal index Xb10, the chromospheric Mg II c/w index, the TIMED SEE 24.07 nm irradiance from the transition region to lower corona, and the F10.7 index. Even though the background X-ray flux is log-transformed (Xb10), it still exhibits logarithmic scaling with respect to the other indices. Normalization rescales the dynamic range but does not alter the underlying logarithmic mapping between index values and solar X-ray irradiance. Figure 22 emphasizes how different 0.1-0.8 nm X-ray flux differs from other solar indices. One suspicious observation is the sudden increase in Xb10 at the start of 1997. Also worthy of note is how F10.7 differs from the other solar indices, for example in years 2000 and 2023.

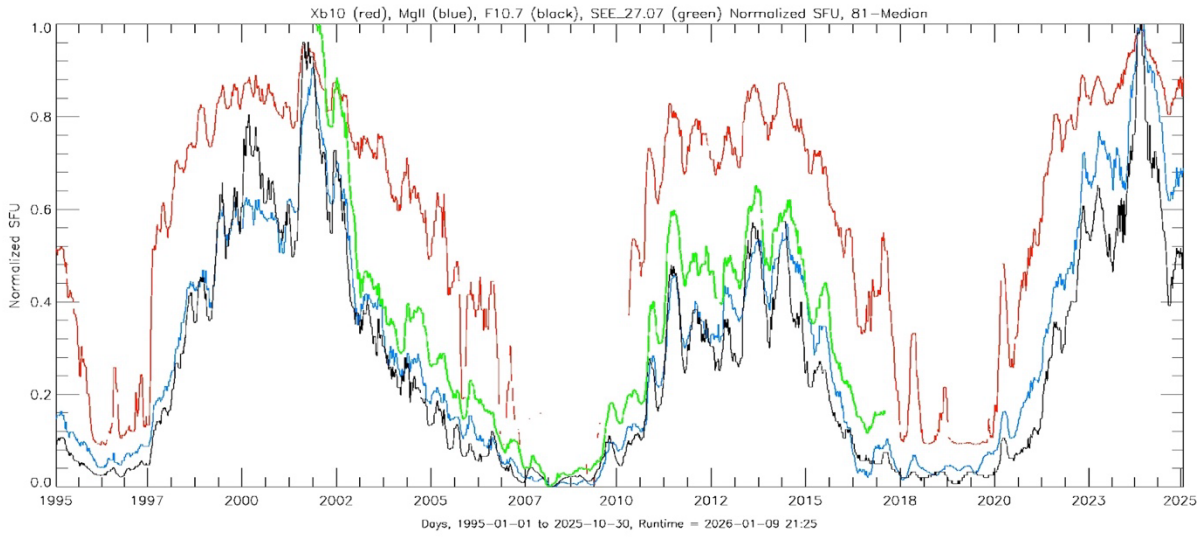

Figure 22. Normalized measurements of Xb10, Mg II, TIMED/SEE 24.7 nm flux, and F10.7 (81-day running median).

Xb10 vs. F10.7

In Figure 23, a quadratic regression was applied. There is a correlation between F10.7 and Xb10, but it is relatively accurate only when solar activity is not dominated by flares, as is apparent in Figure 23 where at high flux levels, the scatter is quite emphasized. Additionally, the effects of the CMD dependence between F10.7 and Xb10 is apparent.

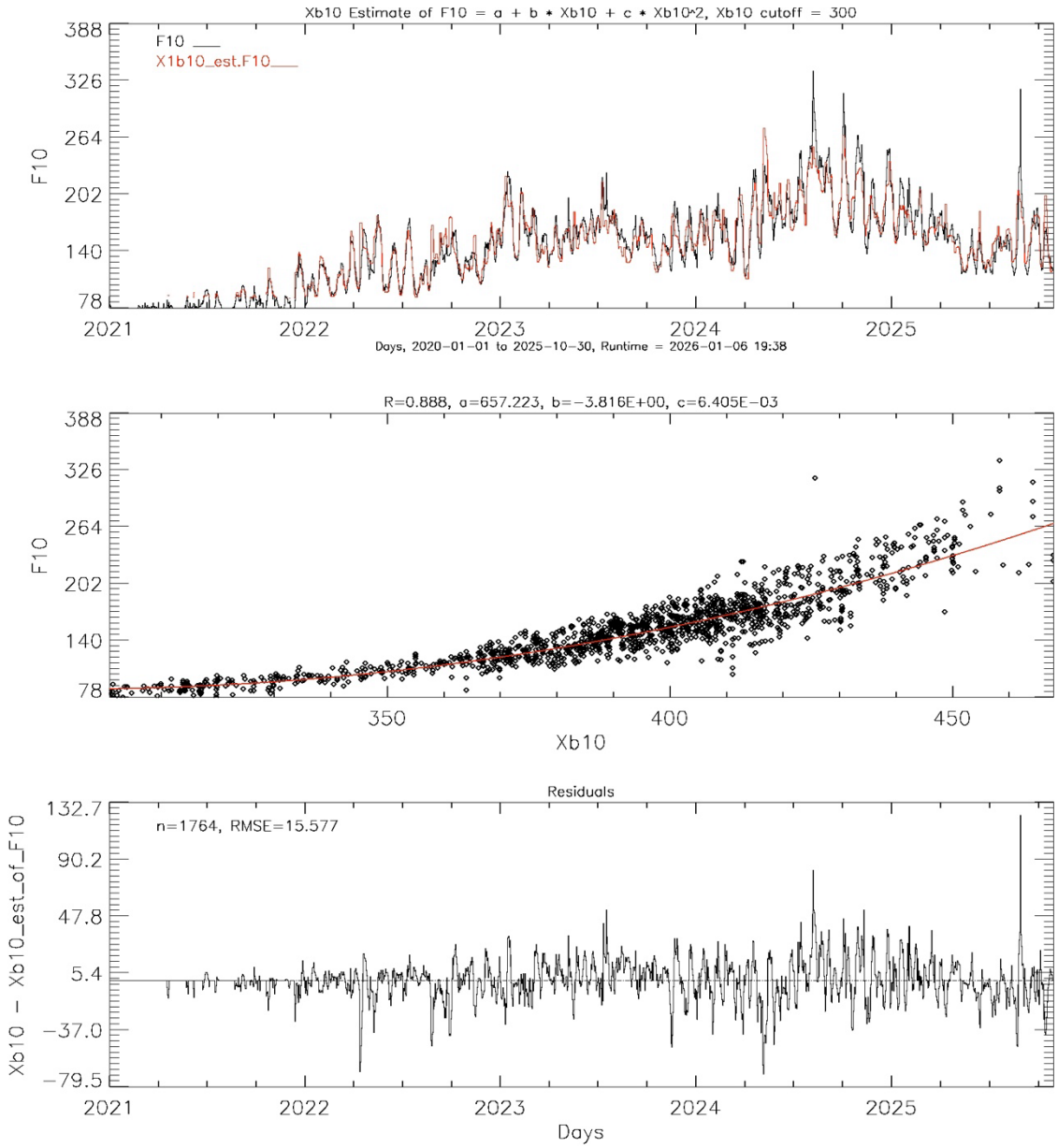

Figure 23. Estimating F10.7 from Xb10 using a quadratic regression, solar cycle 25.

Xhd vs Dst

The Anemomilos Algorithm uses the Xhf flare index, the integrated flux above Xb10, the location (CMD) of the active regions, and solar wind speeds to predict the Dst before it arrives at Earth (Tobiska et. al., 2013). This is illustrated in Figure 24 (Dst is increasingly negative, but plotted here as positive). One particular active region in the northwest quadrant of the sun produced three flares of Xhd > 200, which were related to CME events. Approximately 30 hours later, the Dst reflects the geomagnetic storms at earth, with decreasing influence. Another event occurred earlier between 11/05 to 11/06, during which the CME arrived at Earth only about 18 hours later, underscoring the large variability in solar wind speeds.

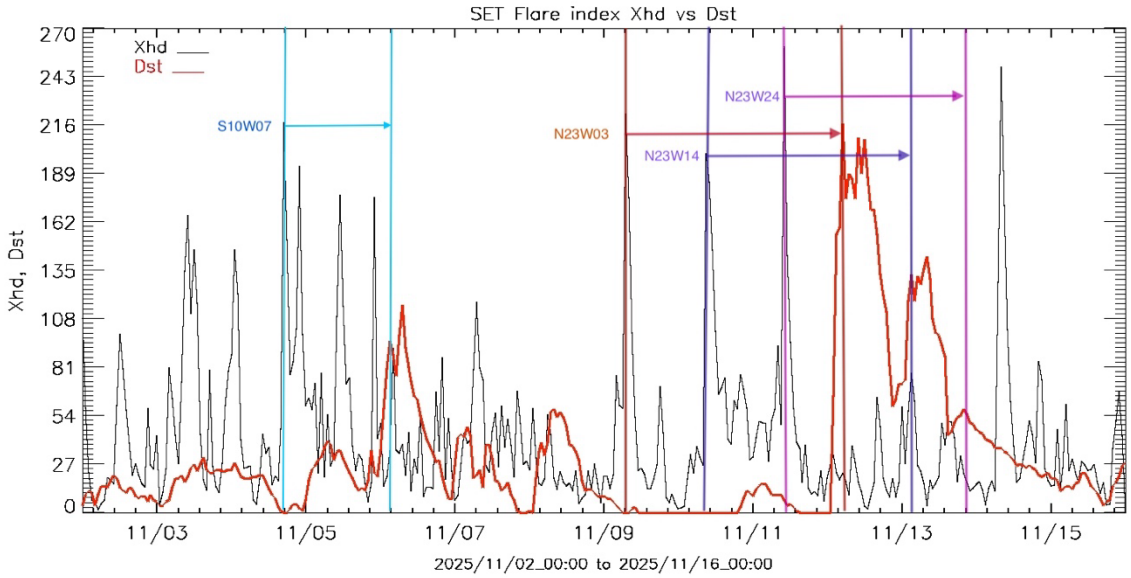

Figure 24. Comparison of Xhd flares with Kyoto Dst, Nov. 2025.

But one surprising result of the Xhd flare index is how it corresponds to the hourly Dst times. An example is shown in Figure 25 for a major geomagnetic storm that occurred May 11, 2024, during which there were numerous X-ray flares. In Figure 25, it is shown that when enhanced Dst is measured at Earth, within an hour or two, if there is a flare occurring, there is a corresponding increase or change in the slope in Dst, possibly related to the effect of increased D-region ionization (*Correia, E., et. al. 2025, Curto, J.J., Gaya-Pique, L.R, 2009*).

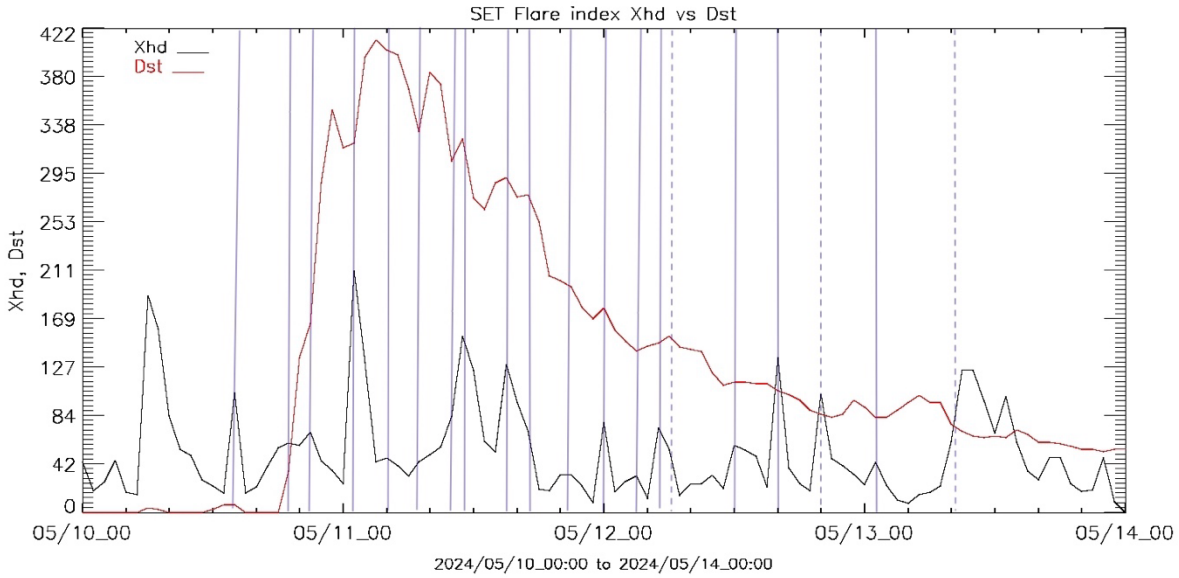

Figure 25. Example of Xhd corresponding to changes to Dst. The negative Dst is shown as positive for illustration.

Conclusion

This project has assembled a single time series of one-minute X-ray data from multiple GOES satellites, providing an integrated, accurate, and accessible database spanning 31 years. The daily background Index Xb10, the lower X-ray flare index Xhf, and the hourly upper flare index Xhd have been produced for solar cycles 23, 24, and 25. An error analysis has been performed, the most reliable GOES XRS data sources identified, and relative errors of X-ray fluxes clarified for other uses. For accurate analytic uses, the lower limit of X-ray flux is 1.2E-7 W/m^2 (Xi=330) is recommended. X-ray indices have been compared to solar F10.7 and geomagnetic Dst indices, providing examples of the applicability of X-ray indices. The availability of data archives has been described.

Appendix A. SET X-Ray Data Archives

Provisional data archives are available on the SET server at
https://sol.spacenvironment.net/spacewx/goes_xrays/.
The data files (e.g., SET_Hist_Daily_Xb10.txt and SET_Hist_Hourly_Xhf.txt) can be used for other studies, with the prior authorization and appropriate acknowledgement:
"Data provided by Space Environment Technologies, Dave Bouwer (dbouwer@spacewx.com, data@spacewx.com)", and refer to this Technical Memorandum:
"SET GOES XRS Solar 0.1-0.8 nm X-ray Flux Data1995 - 2025 (https://spacewx.com)".

See important data restrictions in Appendix B: "Liability and Warranty" at the end of this document.

There is a large collection of all the intermediate and composite files organized as follows in **Table 4**:

Table 4. Final composite and intermediate data and plot files on SET server https://sol.spacenvironment.net/spacewx/goes_xrays/.

Directories	
Composite_XRS_YMDhm_1 min_plots	One-minute composite plot files
Composite_XRS_YMDhm_1 min_data	One-minute composite data files
Daily_Xb10_YYYY_data	Daily x-ray background Xb10 data files
Daily_Xb10_YYYY_plots	Daily x-ray background Xb10 plot files
Hourly_Xhf_YYYY_data	Daily x-ray flare indices Xhf & Xhd data files
Hourly_Xhf_YYYY_plots	Daily x-ray flare indices Xhf & Xhd plot files
SET_Hist_Xb10_Xhf_Xhd	Final Xb10, Xhf, Xhd data and plots
Docs	SET and NCEI documents, tables, figures

References

Bouwer, S.D., et. al. (1982), ***NOAA Tech. Memo. ERL SEL-62. A Summary of Solar 1-8 A Measurements From the SMS and GOES Satellites, 1977-1981***.

Bouwer, S.D., (1983), **Journal of Geophysical Research, Vol 88, No. A10.** ***Intermediate-term Epochs in Solar Soft X-ray Emission***

Bouwer, S. D. (1992), **Solar Physics 142: 365-389**, ***Periodicities of Solar Irradiance and Solar Activity indices, II.***

Bouwer, D. (2006), **SET Technical Report SET_TR2006-002**, ***A Summary of Solar 0.1-0.8 nm X-ray Measurements From the GOES Satellites, 1986-2004.***

Bowman, B. R. (2008), **AIAA/AAS Astrodynamics Specialist Conference, 18-21 August 2008.** ***A New Empirical Thermospheric Density Model JB2008 Using New Solar and Geomagnetic Indices.***

Curto, J.J., Gaya-Pique, L.R., (2009), **Journal of Atmospheric and Terrestrial Physics, Vol.71, Iss. 17-18.** ***Geoeffectiveness of solar flares in magnetic crochet (sfe) production: I***

Correia, E., et. al., (2025), **Advances in Space Research. https://doi.org/10.1016/j.asr.2025.09.032.** ***Characterization of the ionosphere response to the X1.3 solar event occurred on 30 March 2022***

Hyndman, R. & Koehler, A. (2006), **International Journal of Forecasting, *22(4), 679–688*. Another look at measures of forecast accuracy.**

Kreplin, R. W., Taylor, J. A., & Jenkins, H. M. (1970), **Solar Physics, 11**, 184–195. ***Solar X-Ray Emission in the 1–8 Å Band***.

Machol, J. L, et. al. (2026)**. Submitted to Journal of Geophysical Research, 2026.** ***GOES-R Series X-Ray Sensor (XRS): 2. On-orbit measurements and calibrations***.

Montgomery, D. & Runger, G. (2014). **Applied Statistics and Probability for Engineers, 6th ed. Wiley.**

Mothersbaugh, J., Machol, J, Zetterlund, E, A. (2003). ***Readme For Science-Quality GOES-9-15 XRS Data.***
https://data.ngdc.noaa.gov/platforms/solar-space-observing-satellites/goes/goes16/l2/docs/GOES-R_XRS_L2_Data_Readme.pdf

Tobiska, W.K, et. al. (2013). **Space Weather, Vol. 11, Iss. 9.** ***The Anemomilos prediction methodology for Dst.***

Glossary

ASCII - American Standard Code for Information Interchange
CMD - Central Meridian Degree
Dst - Disturbance storm time
DBMS - Database Management System
EUV - Extreme Ultra-Violet
F10 - F10.7 cm (2800 MHz)
FIA - Flare Initiation Algorithm
GHz - GigaHertz
GISS - Goddard Institute for Space Studies
GOES - Geosynchronous Orbiting Environmental Satellite
GPS - Global Positioning System
HASDM - High Altitude Satellite Drag Model
HF - High Frequency
IDL - Interactive Data Language
JB08 - Jacchia-Bowman 2008 (model)
JBH - Jacchia-Bowman Hybrid (model)
Lya - Lyman-alpha
Mg II c/w - Magnesium II center-to-wing ratio
NASA - National Aeronautics and Space Administration
NCEI - National Center for Environmental Information
NESDIS - National Environmental Satellite, Data, and Information Service
NetCDF - Network Common Data Form
nm - nanometers
NOAA - National Oceanic Atmospheric Administration
PE - Percent Error
RMSE - Root Mean Square Error
SET - Space Environment Technologies
SMS - Synchronous Meteorological Satellite
SQL - Structured Query Language
SWPC - Space Weather Prediction Center
TB - Tera-Bytes
TEC - Total Electron Content
UHF - Ultra High Frequency
VHF - Very High Frequency
W/m^2 - Watts per square meter
Xb - Daily X-ray background index
Xb10 - Daily X-ray background index (logarithm base-10)
Xhf - Hourly X-ray flare index
Xhd - Hourly X-ray flare index (highest central tendency, decile-equivalent)
Xi - X-ray index
XRS - X-Ray Sensor

Table of Figures

Appendix B. Data Liability and Warranty

By accessing this website, users of the information provided herein agree to following conditions of Forecast Liability and Warranty.

Space Environment Technologies ("SET") distributes these products as a scientific-based interpretation of possible space weather events in the near future. These products are distributed directly by SET and are protected by United States copyright laws and international treaty provisions. These products are treated like any other copyrighted material such as a book or musical recording.

Secondary commercial distribution of these products is prohibited without the explicit permission of SET. These products may not be rented, leased, or sold to third parties unless a license from SET exists to do so. These products may not be modified, adapted, translated, reverse-engineered, decompiled, or disassembled. Violation of these conditions automatically terminates a right to use these products and all copies must be destroyed.

The products and related documentation are provided "AS IS" and without warranty of any kind. SET EXPRESSLY DISCLAIMS ALL OTHER WARRANTIES, EXPRESS OR IMPLIED, INCLUDING, BUT NOT LIMITED TO, THE IMPLIED WARRANTIES OF MERCHANTABILITY AND FITNESS FOR A PARTICULAR PURPOSE. ANY WRITTEN OR ORAL INFORMATION OR ADVICE GIVEN BY SET, ITS AGENTS, DISTRIBUTORS, OR EMPLOYEES, SHALL NOT IN ANY WAY BE CONSTRUED AS GRANTING OR CREATING A WARRANTY. UNDER NO CIRCUMSTANCES SHALL SET BE LIABLE FOR ANY DIRECT, INDIRECT, INCIDENTAL, SPECIAL OR CONSEQUENTIAL DAMAGES (INCLUDING, BUT NOT LIMITED TO, DAMAGES FOR LOSS OF PROFITS, INFORMATION, OR GOODWILL) THAT RESULT FROM THE USE OR INABILITY TO USE THE PRODUCT OR RELATED DOCUMENTATION, EVEN IF SET HAS BEEN ADVISED OF THE POSSIBILITY OF SUCH DAMAGES.

For U.S. Government users, the technical data products and documentation are provided with technical data LIMITED RIGHTS as defined in DFARS 252.227-7013 and with computer software RESTRICTED RIGHTS as defined in Federal Acquisition Regulation 52.227-14 and DFARS 252.227-7014.

Use, duplication, or disclosure by the all users is subject to the restrictions above. The manufacturer of these products is Space Environment Technologies with address of record located at spacewx.com.